Investigation of Mycobacterial cell wall genes and their requirement for survival in immune related stressful conditions

By

Veneshley Samuels

SMLVEN001

Thesis submitted to the University of Cape Town for the degree (MSc.Med) of Clinical Sciences and Immunology in the Department of Pathology in the Division of Immunology

Supervisor: Ass Prof. Mohlopheni Jackson Marakalala

Co-supervisor: Dr. Hlumani Ndlovu

February 2020

Declaration

I, Veneshley Samuels know that plagiarism is wrong. Plagiarism is to use another's work and pretend that it is one's own.

I have used the Vancouver convention for citation and referencing. Each contribution to and quotation in this thesis from the work(s) of other people has been attributed and has been cited and referenced.

I declare that "Investigation of Mycobacterial cell wall genes and their requirement for survival in immune related stressful conditions" is my own work and that it has not been submitted for any degree or examination in any other university.

This report is my own work. I have not allowed and will not allow anyone to copy my work with the intention of passing it off as his or her own work.

Signature **:** Signed by candidate

Date **:** **09 February 2020**

Acknowledgements

I would like to thank all those who supported me throughout my degree and who made this thesis possible.

I would like to thank the **National Research Foundation** (NRF), **Medical Research Council** (MRC) and **UCT postgraduate funding office** for providing me with financial assistance. I would also like to thank **Professor Valerie Mizrahi** and **the Centre of excellence** for supporting me throughout my studies.

I owe my deepest gratitude to my supervisor**, Ass. Prof Mohlopheni Jackson Marakalala** for allowing me the opportunity to work in his research group. Words cannot describe how grateful I am for having you as my supervisor. Thank you for the endless motivation and words of encouragement. Thank you for giving me the space to do “my thing”. I am not the best at communication, but you consistently kept reminding me that you are always there for me. You are an inspiration and a terrific role model, and I am truly thankful to have been supervised by you.

To my co-supervisor **Dr. Hlumani Ndlovu**, thank you for your guidance, advice, academic support and encouragement. Thank you for always giving me space to run my ideas by you and more importantly, thank you for all the constructive criticism.

To, **Sephekana Mohapi**, “Sammy”, as everyone knows. I am truly grateful for your friendship. Thank you for being a brother, a friend and an amazing colleague. Thank you for making me a music playlist, not just for BSL3 but also for my overnights. Thank you for being there for me and for supporting me through my journey.

To the members in our laboratory, **Welcome**, **Caryn**, **Jamie** and **Stephanie**. Thank you for the support and encouragement. Thank you for all the stimulating discussions and for the great memories.

I would also like to thank **Mr. Avril Walters** for helping me and who pushed me to do my best. Thank you for helping me come over my “fear” in working in the BSL3 laboratories. Thank you for all the time that you invested in training me. Thank you for

making me coffee or lunch and for reminding me that I need to eat. Thank you for being a friend and for keeping me going. Thank you to **Muazzam's** and **Frank's** laboratory for allowing me to work in their space.

To **Dr. Andani Mulelu** and all the members at **Prof Trevor Sewell's laboratory**, I am thankful for your help. Thank you for hosting me at your laboratory and for taking the time to train me on electron microscopy. To **Miranda and Mohammad**, thank you for your patience and for always helping when I went into "panic mode".

I would like to thank **Prof Digby Warner** and his laboratory for always having their doors open for me. To **Audrey Jordaan**, thank you for the patience and the extremely early mornings and late nights "optimizing" MIC assays. Thank you for not only training me, but also for the continuous support, advice and reassurance. I would like to thank **Ditshego Ralefeta** for helping me with fluorescence microscopy, if it wasn't for you, I would not have been able to work after hours to get my work done.

To **Lucas** and **Rendani**, thank you for all the crazy conversations and laughter and for always lending me your student card when I needed access during our "over nights". You have truly made my last few months the most enjoyable.

To my science sisters, **Nontobeko Mthembu**, **Sibongiseni Poswayo** and **Zandile Booi**. All the late nights, unhealthy meals, sunrises, coffee sessions, overnights, sleepovers and "go wishing together", has given me something to be grateful for, and that is true friendship. To **John Iradukhunda** and **Siyabulela Magugu**, I am forever indebted to you for helping me with the 72- and 96-hour experiments. You always have my back.

To my **mother**, **father** and my **grandparents**, words cannot describe my gratitude to you. Thank you for your understanding, your sacrifices, your prayers and your enduring love. To my uncle and aunt **Amolene** and **Lance Louw**, thanks for the encouragement and moral support. I want to thank **Gillian** and **Adley Nel** for welcoming me into their home and for always being there for me when I needed help. To my beloved sister, **Michell**, whenever I panicked and doubted myself, you always reminded me of my achievements. You have encouraged me to never give up. To the

rest of my family members, **Amolia**, **Melvina** and **Chanice** thank you for supporting me, both physically and emotionally.

My sincere thanks to **Mrs. Karen and Mr. Olof Dreyer**, for the unshaken faith, love, time and most importantly the effort and endless patience and kindness. Mrs Karen, you have always been a role model. You inspire me to give my best. Your kind-heartedness has made a huge impact on my life. I will forever be grateful, thank you for being part of my journey

Lastly, I would like to thank my **Lord** and **Saviour Jesus Christ** for giving me the strength to complete my study.

Abstract

Tuberculosis (TB) disease, caused by the pathogen *Mycobacterium tuberculosis* (Mtb), remains a major global health problem claiming 1.5-2 million lives annually. One of the major factors contributing towards Mtb's success as a pathogen is its unique cell wall and its ability to counteract various arms of the host's immune response. Understanding these survival mechanisms will help us develop new therapeutic interventions that can enhance the capacity of the immune system to kill the pathogen. A recent genome scale study profiled a list of candidate genes that are predicted to be essential for Mtb survival of host mediated responses. One candidate was *ftsEX*, a protein complex comprised of an ATP binding domain, FtsE, and a transmembrane domain, FtsX. FtsEX functions through interaction with a periplasmic hydrolase, RipC. FtsEX homologs in other bacteria have been linked to a key role in regulation of PG hydrolysis during elongation and division. Using *M. smegmatis* as a model, we hypothesised that FtsEX and RipC are required in the regulation of PG hydrolysis during normal cell wall elongation and division under stressful conditions *in vitro*. Antibiotic sensitivity was confirmed using Alamar blue MIC determination assays, which showed that *ftsEX* and *ripC* had increased sensitivity to chloramphenicol and not to rifampicin, isoniazid and ethambutol. Our growth curve analysis showed that *ftsEX* and *ripC* are not essential for survival in normal growth conditions. However, *ftsEX* and *ripC* are conditionally essential for *M. smegmatis* in low salt media. Growth defects in this condition were characterized by short and bulgy cells, as well as elongated filamentous cells with visible chaining. Major morphological changes were seen under nitrosative stress. A higher proportion of cells struggled to divide normally and formed chains. Lateral branching was also observed in *ΔftsE*, *ΔftsX* and *ΔftsEX* but not in *ΔripC*. The protein complex was also required for survival in media containing rifampicin. Treatment with the drug exacerbated growth defects of all the mutants, which were much shorter than WT cells, indicating impairment in the elongation process. Collectively, mutants are much shorter in length with an exception of a few extremely lengthy cells, suggesting that ftsEX and ripC are required for both normal cell elongation and division and ultimately for survival in stressful conditions.

Table of Contents

List of figures

Literature review

Methods

Results

Chapter 3

Chapter 4

Chapter 5

List of Tables

Chapter 2

Chapter 3

Abbreviations

ABC transporter	Adenosine triphosphatase binding cassette transporter
ATPase	Adenosine triphosphatase
CLR	C-type lectin receptors
DETA-NO	Diethylenetriamine/nitric oxide adduct
GTPase	Guanosine triphosphatase
HygR	Hygromycin resistance
MIC	Minimum inhibitory concentration
MDR-TB	Multidrug resistant tuberculosis
Mtb	*Mycobacterium tuberculosis*
PAMPs	Pathogen associated molecular patterns
PDIM	Phthiocerol dimycocerosate
PG	Peptidoglycan
PRRs	Pattern recognition receptors
RNI	Reactive nitrogen intermediates
ROI	Reactive oxygen intermediates
TB	Tuberculosis
TDM	trehalose dimycolate
TLRs	Toll like receptors
TRASH	Transposon site hybridization
V-ATPase	Vacuolar Adenosine triphosphatase
WHO	World Health Organization
XDR-TB	Extensive drug resistant tuberculosis

Chapter 1: Introduction

Chapter one: Introduction

1.1 Tuberculosis: Epidemiology

Tuberculosis (TB) remains a major global health challenge and disproportionately affects the most vulnerable strata of society, which is highlighted by the most severe burden of the disease in sub-Saharan Africa (1–3). The World Health Organization (WHO) reported that Africa has one of the highest burdens of TB with an estimated 24% of cases of active TB in 2018 (4). A reduction in active cases to 322000 in 2017 indicates significant advances being made to combat disease progression, however, the rate of mortality remains high with the WHO reporting 1.7 million people succumbing to disease in the same year (5,6). Individuals who are immunocompromised have an elevated risk of developing TB, although the disease also occur in people who are immunocompetent (7).

TB is a contagious disease caused by the inhalation of aerosols containing the aetiological agent *Mycobacterium tuberculosis (Mtb)* (8,9). Majority of people infected with *Mtb*, remains asymptomatic in a state referred to as latent TB (10). Up to one third of the world's population is latently infected and present no risk of transmitting *Mtb* (11). Similarly, these individuals do not experience adverse health effects but do face an on-going risk of developing active TB upon reactivation (12). Progression to active TB can occur if the host's immune system is unable to contain the infection. Active TB is symptomatically associated with chest pains, loss of appetite, excessive sweating, difficulty breathing, fever and haemoptysis. If multiple symptoms occur, the disease may lead to physical exhaustion and debilitation.

The standard first line treatment for TB consists a regimen of rifampicin, isoniazid, pyrazinamide and ethambutol (5,13,14). Adherence to treatment is crucial for anti-TB therapy to be effective. However, the situation of TB disease is worsened by the emergence of multidrug resistant (MDR) strains of *Mtb* (15). MDR-TB is when strains of *Mtb* have resistance to at least rifampicin and isoniazid, which are the two key drugs in the treatment of the disease (15). MDR-TB is treated with second-line drugs, a regimen comprised of fluoroquinolones (levofloxacin, ofloxacin, ciprofloxacin and

moxifloxacin), injectable drugs (capreomycin, kanamycin and amikacin), as well as ethionamide, cycloserine, prothionamide, p-aminosalicylic acid and terizidone (15).
A more serious form of MDR-TB is extensively drug resistant (XDR-TB), which is defined as resistance to rifampicin, isoniazid and at least one drug in both classes of the second-line regimen, namely, fluoroquinolones and injectables drugs (16,17). XDR-TB is rare, however reliable evidence shows that 6,2% of MDR-TB cases progress to XDR-TB (18). Although a small proportion of XDR-TB cases have been reported, resistance is one of the reasons why the disease has not been better controlled until today (18–20).

1.2 Innate defences: Macrophages vs Mtb

TB is a pulmonary infection since the pathogen primarily invades the lungs. The innate immune response against *Mtb* comprises of an aggregation of neutrophils, dendritic cells, alveolar macrophages and CD4-T lymphocytes that work in concert to form a granuloma which is a defensive structure that was initially thought to “wall off” and contain the pathogen (21,22).

Macrophages form the first line of defence in eliminating *Mtb* and are armed with several immune effector mechanisms capable of both detecting and combating the invading pathogen (23,24). However, *Mtb* is able to survive within the phagosome of resting macrophages (25). Upon arrival of adaptive immunity, macrophages are activated by CD4 T cells that release effector cytokines such as IFN-γ (26). After activation, macrophages possess a more potent antimicrobial arsenal that includes phagosome maturation, phago-lysosome fusion as an intoxication mechanism via acidification, production of reactive oxygen and nitrogen intermediates (ROI, RNI) and nutrient starvation (figure 1) (24,27). While all of these effector mechanisms pose a threat for intracellular survival of Mtb, mycobacteria have been shown to express genes that prevent phagosome maturation events and subvert the killing effect of the macrophages.

One of the first macrophage-mycobacteria interactions is the binding of the pathogen through macrophage pattern recognition receptors such as Toll-like receptors (TLRs)

and C-type lectin receptors (CLRs) (28). These receptors are activated by pathogen molecular patterns (PAMPs), which are present on the pathogen (29). *Mtb* possesses surface PAMPs such as the glycolipid trehalose dimycolate (TDM), mannosylated lipoarabinomannan, peptidoglycan, phosphatidylinositol mannosides (28). *Mtb* also expresses a surface lipid called phthiocerol dimycocerosate (PDIM), which masks PAMPs to evade recognition by the host immune response (29). Furthermore, PDIM is actively produced and secreted during mycobacterial infection and is under the control of a regulatory protein called WhiB3 (30). PDIM has also been identified as one of the lipid groups produced by WhiB3 to function as a reduction sink when faced with macrophage induced reductive stress. PDIM is one example of the "underestimated manipulative roles" of how *Mtb* exploits the host immune response in its favour (31).

A key trait and also one of the most well studied evasion mechanisms of *Mtb* is the ability to inhibit phagosome maturation and ensure survival and replication (32). Phagosome membranes have vacuolar-H^+-ATPase(V-ATPase) machinery responsible for acidification, however, *Mtb* secretes a protein that directly binds host V-ATPase to dephosphorylate and inactivate it during infection (33,34). Another tactic that has been identified is *Mtb's* alternate adaptation mechanism (35). *Mtb* outsmarts the immune system by activation of host cytosolic phospholipase A_2, to escape from phagosomes and establish infection in the cytoplasm of the cell (35) . In addition, *Mtb* has been shown to counteract effects of amino acid starvation in activated macrophages. The pathogen normally utilizes the host tryptophan as a nutritional source. However, it turns to its own tryptophan synthetic genes, trpE and trpD, when starved of the host amino acid in activated macrophages (26). Thus, starvation also "fails as an *Mtb*-killing mechanism" (26). While more research is still needed to understand *Mtb*'s evasive mechanisms in detail, the above-mentioned examples suggest that *Mtb* has evolved various strategies of evading or subverting normal host defences (36).

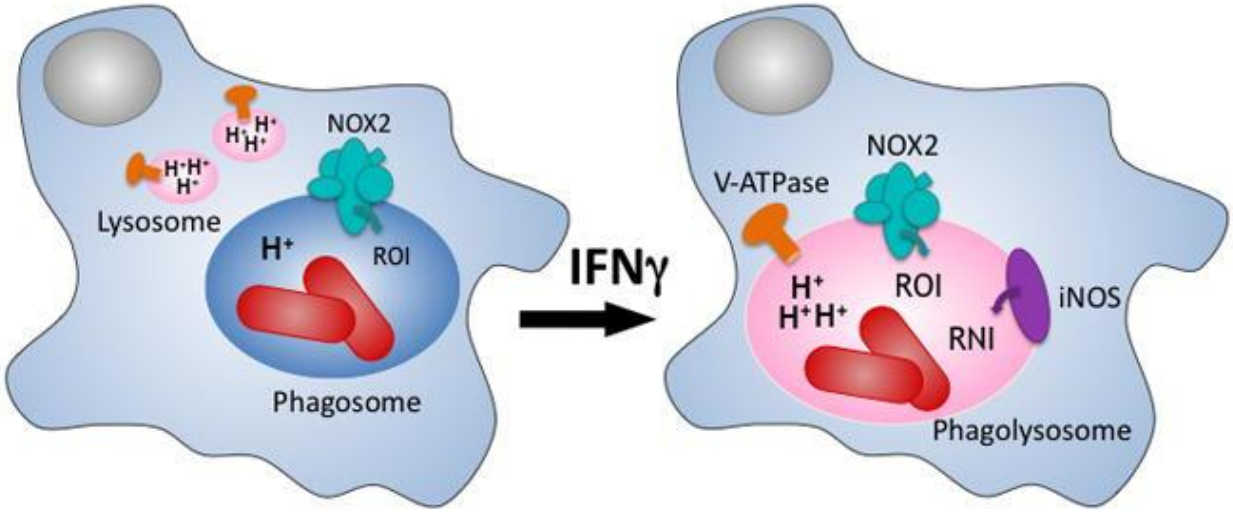

Figure 1. **Macrophage defences against *Mycobacterium tuberculosis* (*Mtb*).**

Mycobacterium tuberculosis **(***Mtb*) is stalled in the phagosome, as a result it resides in a mildly acidic environment. Phagosome maturation and fusion with lysosomes occurs as a result of activation with IFN-γ. Consequently, *Mtb* becomes exposed to protons from the vacuolar ATPase, ROI from NOX2 and reactive nitrogen intermediates (RNI) from inducible nitric oxide synthase(iNOS). (Image adopted from (34)).

1.3 Unravelling the structure of the mycobacterial envelope

Among the factors that contribute to *Mtb's* success as a pathogen is its ability to withstand potentially bactericidal host defences and to resist elimination by an activated immune system (37). *Mtb* owes much of its success to its unique cell wall (figure 2) (11). Described as unusual, the cell wall has an inner and outer layer (37,38). The outer layer is dominated by essential lipids, proteins and carbohydrates that form an efficient permeability barrier which plays an important role in drug resistance and also survival of during stress conditions in inside macrophages (38,39). The inner compartment contains three distinct macromolecules; a characteristic long chain mycolic acid layer, a highly branched arabinogalactan and a glycan peptide cross linked network of peptidoglycan (PG) (38).

All bacteria encounter common challenges during proliferation where normal cell wall architecture needs to be maintained before, during and after cell division (40). Because of the complexity of the mycobacterial cell wall, many layers must be synthesized which requires careful regulation (3,40). During division and elongation of *Mtb*, a coordinated cell wall regulation is fundamental for the incorporation of newly

synthesized cell wall material (3). As a result, a continuous PG sacculus is formed in a spatially defined manner and becomes hydrolysed at the correct time and place allowing daughter cells to separate (3). The PG layer is therefore essential and an important component of the cell envelope because it undergoes dynamic remodelling by providing the necessary strength and rigidity when bacterial division occurs and when *Mtb* becomes exposed to environmental stresses (3,41).

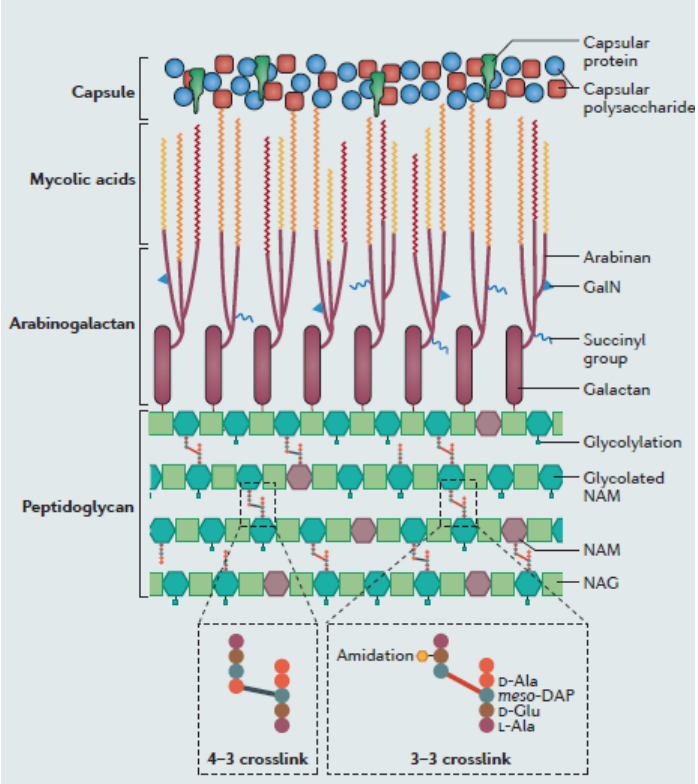

Figure 2. **Cell wall envelope of mycobacteria.**
Mycobacteria have a complex cell wall structure which is required for cell growth, virulence and antibiotic resistance. It is made up of three distinct macromolecules: peptidoglycan, arabinogalactan and mycolic acids**.** Peptidoglycan is the most fundamental layer which consists of repeated alternating sugars N-acetyl glucosamine (NAG) and NA/MA (muramic acid) forming glycan-peptide crosslinks responsible for maintaining cell shape, size and functioning in cell wall regulatory processes such as hydrolysis. Image adopted from (11).

1.3.1 Peptidoglycan Hydrolysis

Hydrolysis of PG is performed by amidases/hydrolases/peptidases, a group of enzymes that remove stem peptides from the glycan strands of PG (figure 3) (42).

Hydrolases specifically cleave each bond in PG ultimately breaking the cross-links (41). How bacteria ensure that PG hydrolases function only in the correct spatial and temporal context remains largely unknown. However, several studies have demonstrated how dysregulation of this homeostatic balance has lethal effects on the bacterium causing lysis of the cells (42). Furthermore, unchecked PG hydrolysis can alter the division process and cells can form long chains (43–45). It is therefore important to understand the cellular mechanisms regulating this structurally controlled dynamism that needs to be maintained to prevent breaches in cell wall integrity (3,42).

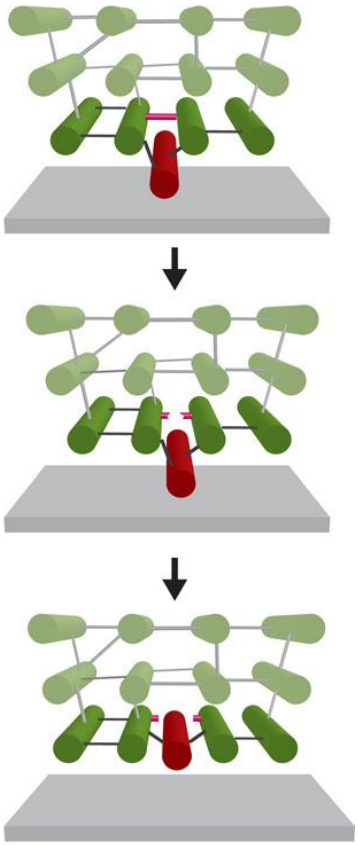

Figure 3. **Schematic 3-dimensional diagram of peptidoglycan synthesis.**
The PG layer is adjacent to the cell membrane (grey surface). The PG layer is shown in dark green. A newly synthesized glycan strand is shown in red and is cross-linked to adjacent older strands. Peptide bonds are cleaved as shown in hot pink. This is followed by incorporation of the new strand into the existing layer. (Image adopted from (50)).

1.3.2 The link between PG hydrolysis and cell division

A model emerging from recent work is that PG hydrolases are auto-inhibited and require interactions with regulatory proteins which form large macromolecular complexes in the cell envelope (46). These complexes in turn, are coupled to the cell division apparatus responsible for coordinating both synthetic and hydrolytic activities. PG hydrolases accordingly require interactions with regulatory proteins but their genes show high redundancy which makes it difficult to assign distinct roles (3,47).

For successful growth of *Mtb*, a normal architecture needs to be maintained, breakdown of cell wall components needs to be coordinated through hydrolysis, and cell division needs to be regulated in response to environmental stimuli (40). A central problem is understanding how signalling events inside the cell stimulate PG hydrolysis outside the cell (3). The most clearly defined septation event occurring in almost all bacteria is polymerization of the self-activating GTPase protein, FtsZ (3,48). FtsZ protein, when catalysed, results in the formation of a circumferential Z-ring (figure 1.4) (3,49,50). Z-ring formation is a critical early event during bacterial division, determines the site of septation and acts as a scaffold by recruiting and coordinating multi-protein complexes that enhance septation (3,11).

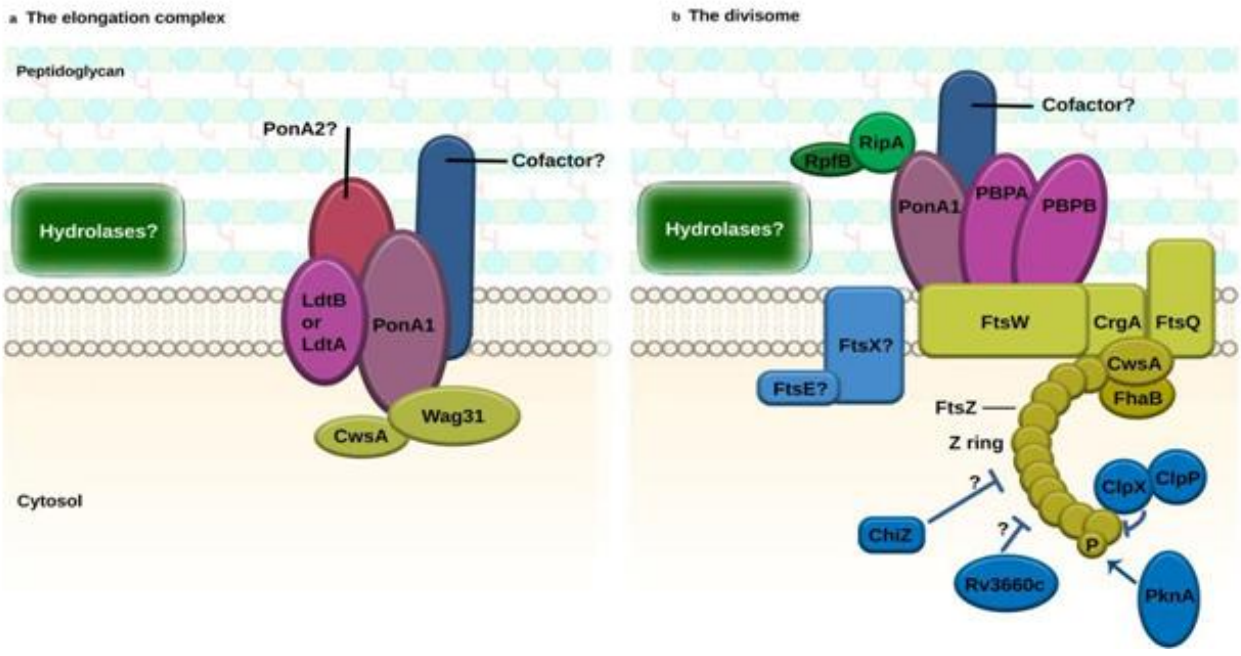

Figure 4. **Multi-protein complexes involved in elongation during cell division.**

Large macromolecular complexes comprising of regulatory factors/proteins (blue), peptidoglycan hydrolases (green), structural proteins (yellow) and peptidoglycan synthases (pink). A, Represents the multi-protein elongation complex responsible for driving polar elongation. B, Represents the divisome responsible for regulating cell division. (image adopted from (11))

1.3.4 Protein machineries direct cell growth and division

Since the functions of many of the components in the multi-protein machinery are still undefined, the challenge is to understand the mechanisms that mediate cell division processes (51). An emerging model is that FtsEX form one such complex which senses the progress of division and regulates extracellular PG hydrolases (3). The general structure of FtsEX resembles that of ABC transporters (ATP binding cassette); proteins that use ATP as the form of energy to transport different substrates/molecules either into or out of cells (52). Current literature however describes FtsEX as a combination of a cytoplasmic ATPase protein, FtsE, and a transmembrane protein, FtsX (figure 4) (3,46,53). FtsE is a putative protein possessing Walker A and B motifs known to bind and hydrolyze ATP. FtsX is composed of large and small extracellular looping domains that span the membrane and interact with a PG hydrolase in the periplasmic space (3,51). Interestingly, FtsEX has been implicated as an important contributor to *Mtb's* evasion of CD4-mediated immune responses in a genome-wide transposon site hybridization approach (TRASH) (26).

1.3.5 FtsEX is widely distributed amongst other bacteria

FtsEX has been found to be important for cell division and growth in other bacteria such as *Escherichia coli*, *Streptococcus pneumoniae and Bacillus subtilis* where it has been shown to be either essential or conditionally essential (49,50,52). To coordinate septum formation in *E. coli*, 12 proteins localize in an independent sequential manner to form a multi-protein complex at the mid-cell (54). Upon cytokinesis, the periplasmic amidases AmiA, AmiB and AmiC mediate septal PG splitting (3,51). Amidases alone are weakly active enzymes, so they require specific activation by divisome associated proteins that carry LytM domains (54,55). Activation of AmiA and AmiB occurs through the LytM domain protein, EnvC, while AmiC is activated by NlpD (51). How LytM

domain proteins are controlled and how they in turn control amidase activity remain poorly understood.

Earlier work on *E. coli* implicated FtsEX in division, however, this was challenged because division defects in ftsEX mutants are salt remedial (52). This means that cell viability is restored upon inclusion of salt (NaCl) in growth medium; hence, it is conditionally essential for survival. Subsequent work by Yang et al, 2011 demonstrated the direct recruitment of FtsEX by EnvC (figure 5). They showed that mutations in FtsEX phenocopy cell separation defects of EnvC mutants and were synthetically lethal, suggesting that FtsEX and EnvC participate in the same biochemical pathway (51).

In the gram-positive pathogen *S. pneumoniae*, the putative CHAP domain protein, PcsB, emerged as the candidate PG hydrolase. Like EnvC and NIpD, PcsB interacts with FtsX through a predicted N-terminal coiled-coiled domain (49). Although differences in shape and PG synthesis patterns exist between *E. coli* and *S. pneumoniae*, evidence consistently shows that depletion of ftsEX generates cell morphology defects (3,49). The role of FtsEX as a regulator of PG hydrolase activity seems to be conserved across bacterial species. In *B. subtilis,* FtsEX regulates two functionally redundant DL-endopeptidases LytE and CwlO (50). In cells depleted of both these enzymes, PG synthesis continues to move circumferentially but eventually result in cell lysis (50). These results suggested that FtsEX, in the case of *B. subtilis* is non-essential, but overall suggest a model in which the complex might serve as a flexible regulator required for the control of diverse PG hydrolases in different bacterial species (3,49,50,53,54).

To understand the role of FtsX in the divisome and its mechanism of PG regulation in mycobacteria, Mavrici et al, 2014 characterized the interaction between FtsX and extracellular enzymes. The authors managed to define the enzyme partner interacting with the larger extracellular loop of FtsX. In the model, they showed that FtsX interacts with the PG hydrolase, RipC (figure 5). The FtsX-ECD crystal structure revealed a binding site for RipC, which was described as a hydrophobic cleft containing two domains (3). Mutations in the amino acid residues in the cleft completely abolished RipC binding, indicating that RipC binding is functional (3). The biochemical and

structural studies provided by these findings therefore gives us insight into understanding the mechanism of bacterial growth during *Mtb* infection.

Not much is known about the role of FtsEX in mycobacteria, especially when the bacterium is exposed to host immune and antibiotic stressors. We hypothesized that FtsEX in *Mycobacteria* is involved in the regulation of cellular elongation and division particularly when the bacterium is exposed to host immune and antibiotic stressors. Hence, the main aim of this study was to clone and generate different mutants of *M. smegmatis ftsEX-ripC* gene complex and to investigate their protective role in immune related stressful conditions *in vitro*.

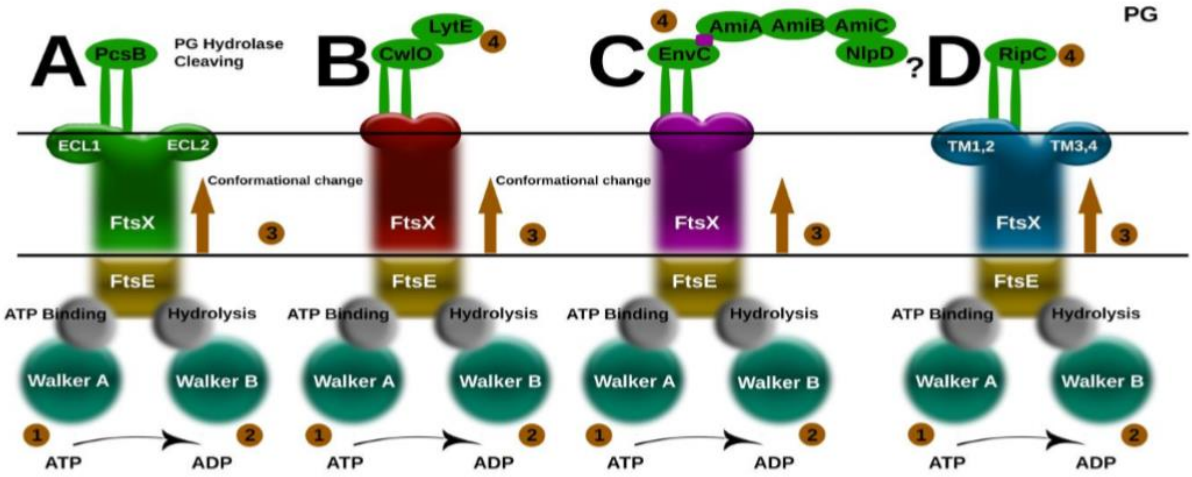

Figure 5. **Schematic representations of model(s) for regulated PG hydrolysis show homology in various bacteria.**

The FtsEX complex share structural similarities to an ABC transporter, however its function is coupled to PG hydrolysis. FtsEX is a combination of a transmembrane protein FtsX and a cytoplasmic ATPase FtsE. FtsX contains a large extracellular loop domain, ECL1, and a small extracellular loop domain ECL2 (shown as TM1, 2 and TM3, 4, D-*M. tuberculosis*). A, FtsEX: PcsB complex *in S. pneumoniae*. ECL1 interacts with the coiled -coiled domain of the PG hydrolase PcsB. PcsB is activated through the ATPase activity of FtsE, which in turn drives conformational changes in the transmembrane domain of FtsX. Conformational changes in FtsX is transmitted through the extracellular loops, ECL1 and ECL2, which is predicted to relieve auto-inhibition of the PcsB CHAP domain (not shown), therefore allowing timed PG cleavage. B, FtsEX: CwlO complex in *B. subtilis*. C, FtsEX: EnvC-NlpD complex in *E. coli*. D, FtsEX: RipC complex in *M. tuberculosis.*(adopted from (3,49,50,52)).

1.4 Rationale

What makes TB disease a problem is that causative agent, *M. tuberculosis*, possesses unique mechanisms that subvert the killing effects of the host immune response. Therefore, in order to solve this problem, one would need to understand how mycobacteria work against host defences. Our research focuses on a cell wall protein complex called FtsEX and a periplasmic amidase called RipC. We considered studying these genes because it was predicted by a genome wide transposon site hybridization (TRASH) approach to be required for *Mtb* survival in a CD4 mediated immune stem. What makes it more interesting is that FtsEX has homologs in other bacteria where it is also associated with periplasmic amidases. Hence, FtsEX seem to play a conserved regulatory role. Moreover, these findings suggest a common paradigm that might be essential to maintain normal cell elongation and division in bacterial species including Mycobacteria and can therefore be targeted for drug designing.

1.4.1 Main Hypothesis

It is hypothesized that mycobacterial FtsEX and RipC are involved in the regulation of cellular elongation and division particularly when the bacterium is exposed to host immune and antibiotic stress.

1.4.2 Objectives of the study:

- To clone and construct *M. smegmatis ftsEX-ripC* mutants.
- To determine the sensitivity of *ftsEX* and *ripC* mutants to anti-TB drugs using the Alamar Blue Assay.
- To investigate the conditional essentiality of *ftsEX* and *ripC* by exposing mutants to various *in vitro* stresses that mimic an intracellular macrophage environment.
- To analyse phenotypes related to cell division and septation using scanning electron and fluorescence/confocal microscopy.

Chapter 2: Methods

Chapter two: Methodology

2.1 Polymerase Chain Reaction Primer (PCR) design

Genomic sequences for *Mycobacterium smegmatis (M. smegmatis)* MC^2155 genes *ftsE* (MSMEG_2089), *ftsX* (MSMEG_2090), *ftsEX* (MSMEG_2089-2090) and *ripC* (MSMEG_4256) were obtained using Mycobrowser, a genomic and proteomic data repository for mycobacteria. Two sets of primers were designed to target about 500bp regions upstream and downstream of the target genes. Primers were analysed using OligoAnalyzer tool hosted by Integrated DNA technologies (IDT). The widely used program assessed primers on the following: melting temperature (Tm), length, GC content, and the likelihood of self-dimer and secondary structure formation. The primers also have sequences complimentary to a hygromycin resistance gene that was used for overlap extension PCR/Stitch PCR with the amplified upstream and downstream regions (figure 2.1). Primers were manufactured by the Molecular and Cell Biology Synthetic DNA laboratory at the University of Cape Town and IDT.

2.1.1 Construction of *M. smegmatis* knockout strains

About 500bp of upstream and downstream flanking regions of the genes *ftsE*, *ftsX*, *ftsEX* and *ripC* were amplified from the genomic DNA of *Mycobacterium smegmatis* MC^2155 using Gotaq® DNA polymerase (Promega, United States) PCR approach (3). Flanking sequences were produced from a 40µL reaction volume containing the following: Gotaq master mix, DMSO, forward and reverse primers, genomic DNA and dH_2O (table 1). The PCR reactions were performed using the SimpliAmp thermal cycler (ThermoFisher Scientific, South Africa) program as in figure 2.2. Following amplification, amplicons were further analysed by agarose gel electrophoresis, purified using the Wizard® SV Gel and PCR Clean up system (Promega, Wisconsin, USA) and quantified by Nanodrop (Fluoroskan Ascent NP-1000, ThermoFisher). All purified PCR amplicons were stored at 4^0C.

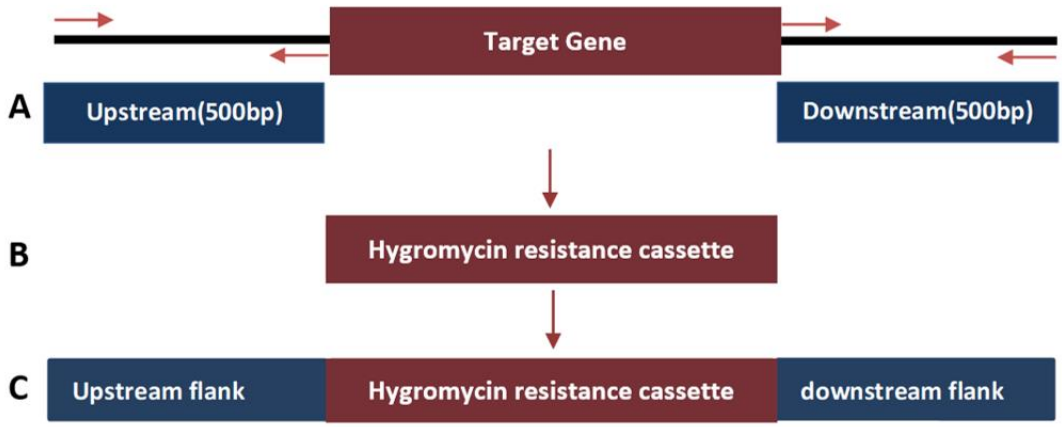

Figure 2. 1. **Schematic diagram illustrating different PCR reactions and expected PCR products.** (A) Expected products for upstream and downstream flanking regions of 500bp genes *ftsE, ftsX* and *ripC*. (B) Expected product for hygromycin resistance gene cassette of 1200bp, to be stitched between flanking regions. (C) The product expected from the stitch PCR reaction of 2200bp.

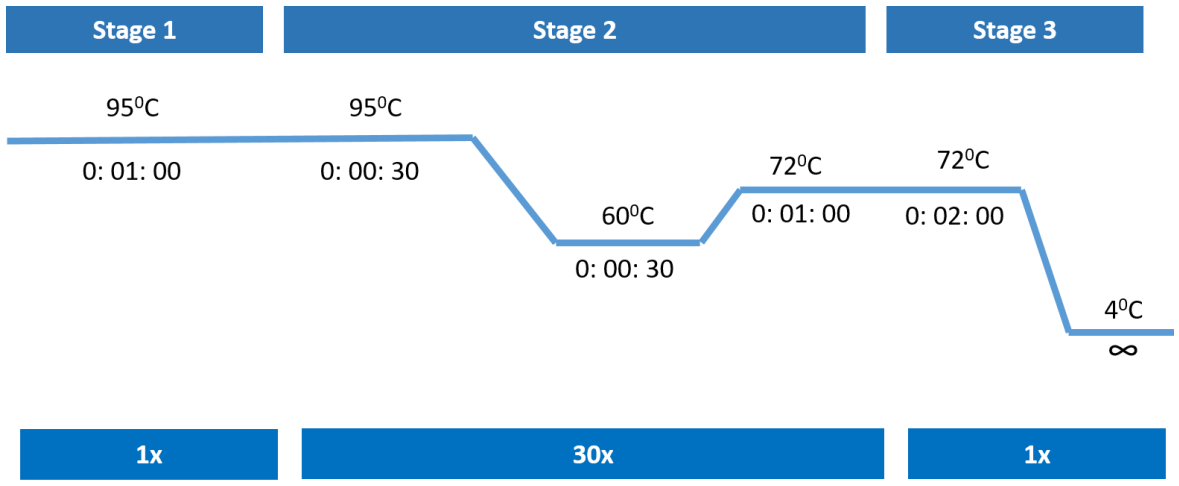

Figure 2. 2. **Gotaq approach used for PCR reaction(s).**
Schematic view of Gotaq approach used for amplification of genes *ftsE, ftsX, ftsEX, ripC* and hygromycin resistance cassette.

Table 2. 1. **Samples and reaction mix used for PCR amplification of *ftsE, ftsX, ftsEX and ripC* flanking regions**

Samples	Sample 1	Sample 2	Sample 3	Sample 4
Reaction Mix	FtsE	FtsX	FtsEX	RipC
1. **Gotaq**	20 µL	20µL	20 µL	20 µL
2. **DMSO**	3,5 µL	3,5 µL	3,5 µL	3,5 µL
3. **PRIMER F**	1 µL	1 µL	1 µL	1 µL
4. **PRIMER R**	1 µL	1 µL	1 µL	1 µL
5. **gDNA**	1 µL	1 µL	1 µL	1 µL
6. **H_2O**	13,5 µL	13,5 µL	13,5 µL	13,5 µL

2.1.2 Agarose gel electrophoresis

PCR amplicons were analysed by electrophoresis on a 1% (w/v) agarose gel in 1× TBE buffer. The amplicons were loaded on a gel alongside a 1kb or 100bp DNA ladders and run for 1h at 100V using BIO-RAD Model 250/2,5 power system. The products (amplicons) were visualized under ultra-violet (UV) light using the Syngene g: box (Vacutec, California, USA).

2.1.3 Amplification of 1200bp Hygromycin resistance cassette

A PCR was performed to amplify a hygromycin resistance cassette of 1200bp. The HygR cassette was previously inserted into a TOPO® plasmid and was amplified using primers MJ.156 (forward) and MJ.157 (reverse) (table 2.2) using the Gotaq protocol (figure 2.2).

Table 2. 2. **Sequences of primers used to amplify *M. smegmatis ftsE, ftsX, ftsEX* and *ripC* 500bp flanking regions**

Name	Purpose	Sequence
VS.001	FtsE upstream F primer	GTGCTGATCGTGGCGTTCTTC
VS.002	FtsE upstream R primer	CTA CTT GTC GTC GTC GTC CTT CTT GTA CTG CTT CGT CAC GTG G
VS.003	FtsE downstream F primer	GTT TTT TTG GGC CTA GGG AAG G GTGATGAACAGCGCGGCGTC
VS.004	FtsE downstream R primer	CAA GTC CTT CTG GTT GAG CAC G
VS.005	FtsX upstream F primer	TCA ACA AGC TGC CCG GCC
VS.006	FtsX upstream R primer	CTA CTT GTC GTC GTC GTC CTT GCCCGGTCAGGACTTCATTGA
VS.007	FtsX downstream F primer	GTT TTT TTG GGC CTA GGG AAG G GTG ACA CTG CGG CTG TAC GT
VS.008	FtsX downstream R primer	GCT CGC GGA TCA CCT CGC
DM.01	RipC upstream F primer	TCC CGT CTC ACA GGA AGT CA
DM.02	RipC upstream R primer	CTA CTT GTC GTC GTC GTC CTT GTG CCT CAA GTT TTC GTC CTC A
DM.03	RipC downstream F primer	GTT TTT TTG GGC CTA GGG AAG GTG TGC TGC TGG TCG AAC
DM.04	RipC downstream R primer	TGG TGA TCG CGG CGA TGT
MJ. 156	HygR downstream F primer	CTA CTT GTC GTC GTC GTC CTT GCC GAC GAT TTG TAC TGC TTG G
MJ. 157	HygR upstream R primer	GTT TTT TTG GGC CTA GGG AAG GGC TGG TAC GCG ACG AAC AGC

2.1.4 Overlap extension PCR: construction of 500bp-HygR-500bp stitched products

The hygromycin resistance (HygR) cassette of 1200bp was stitched between 500bp flanking regions of the genes *ftsE*, *ftsX*, *ftsEX* and *ripC* using overlap extension/stitch PCR. Stitch PCR has two main steps: (1), annealing of the PCR products (500bp upstream and downstream flanking regions) to the 1200bp HygR resistance cassette using the KOD Xtreme Hot Start DNA polymerase PCR (Merck, South Africa) approach (figure 2.3); (2) amplification of the stitched products using the Gotaq approach in figure 2.2. All PCR amplicons were examined as previously described. A marker of 1kbp DNA ladder was used to validate successful stitch product sizes that were expected to be between 2000-2200bp.

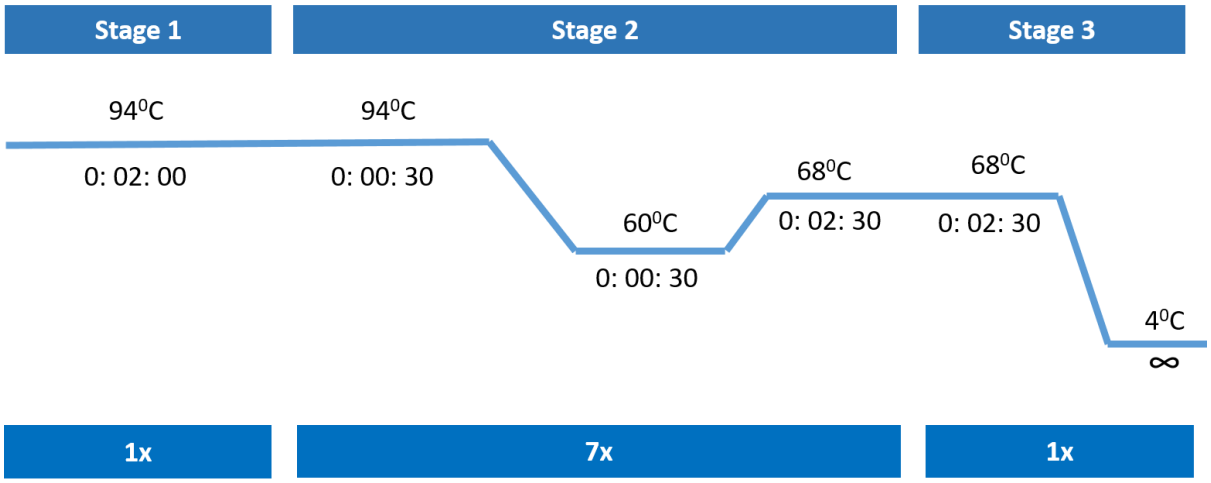

Figure 2. 3. **KOD Hot start/ Stitch PCR approach used for PCR reaction(s).**
Schematic view of KOD approach used to stitch 500bp flanking regions of the genes *ftsE, ftsX, ftsEX* and *ripC* with 1200bp hygromycin resistance cassette.

2.2 pJV53 Plasmid Isolation

Escherichia coli (*E. coli*) DH5-α cells containing pJV53, an acetamide inducible recombineering plasmid, were cultured at 37^{0}C in Luria-Bertani (LB) medium containing kanamycin (25µg/ml). Cultures were grown to an OD of 0,6-0,8 and the plasmid was purified/isolated using the PureYield™ Plasmid Miniprep System

(Promega, Wisconsin, USA). Plasmid DNA was measured by Nanodrop and stored at 4^0C.

2.2.1 Transformation: Preparation of *M. smegmatis* MC^{2}155 pJV53 recombinase strain

The transformation procedure was modified from the Bio-Rad research laboratories protocol (56). *M. smegmatis* MC^{2}155 cells were grown to an OD of 0,8-1,2. Following 1,5hr incubation on ice, cells were harvested by centrifugation at 4000rpm for 10min at 4^0C and washed in an equal volume of ice cold 10% glycerol. Cell pellets were washed in 10ml and 50ml 10%glycerol for 10 and 15min and centrifuged as above. Pellets were re-suspended in a final volume of 1ml 10% glycerol. 50-100µL of the cells were gently mixed with 5µL (5µg/µL) of plasmid DNA (pJV53) and incubated on ice for 1min. For transformation, one pulse at 2.5kV,1000Ω, 25µF time constant 15.0-25.0msec was delivered using the Nucleofector™2b device (Lonza). Electroporated cells were allowed to recover in Middlebrook 7H9 media for 2-4hrs at 37^0C and plated on 7H10 agar with kanamycin (25µg/ml).

2.2.2 DNA recombination: Growth and preparation of pJV53 *M. smegmatis* and KO strains

The acetamide inducible *M. smegmatis* MC^{2}155 pJV53 recombinase strain was cultured for recombination of the hygromycin containing stitched constructs using standard *M. smegmatis* recombineering protocol (Ref). Briefly, *M. smegmatis* MC^{2}155 pJV53 was grown to an OD of 0.65-0.8 in complete Middlebrook 7H9 media containing kanamycin (25µg/ml). Acetamide (inducer, 0.2% m/v) was added to the culture and left to incubate with shaking at 37^0C for 3 hrs. Cells were washed and centrifuged 2-3 times at 4000rpm for 10 min. The pellet was re-suspended in a 1/10th volume of 10% glycerol. For electroporation, 5µL (1µg/µL) of purified DNA of the 500bp-HygR-500bp stitch products was mixed with 400µL of cells and pulsed at 2.5kV,1000Ω, 25µF time constant 15.0-25.0msec. After electroporation, cells were transferred into 4ml 7H9 media (no antibiotic) and incubated with shaking at 37^0C for 3hrs. Following

incubation, cells were plated and selected on 7H10 agar containing hygromycin (50µg/ml) and kanamycin (25µg/ml).

2.3 Colony PCR

After selection on 7H10 agar, clones were screened for targeted band size using colony PCR. Single colonies were picked and grown in 7H9 media containing hygromycin and kanamycin. Cultures were then streaked on 7H10 agar containing 50µg/ml hygromycin and 25µg/ml kanamycin before PCR validation using the Gotaq approach. Individual clones were picked and used as a template for colony screening of the presence of hygromycin cassette (1200bp) with primers MJ.156 and MJ.157 (table 2).

2.4 Drug susceptibility testing by Minimum Inhibitory Concentration (MIC_{90}) determination

The ability of *M. smegmatis* MC^2155 wildtype (WT) and mutant strains to survive antibiotic stress was determined using the Alamar Blue protocol/broth micro dilution method modified from Franzblau et al., 1998 and Jorgensen et al., 2007. Cultures of the relevant strains were grown to an OD_{600} of 0.6-0.8. The plate layout is a modification of the method previously described by Ollinger et al., 2013 using a round bottom 96 well plate. Controls used were a minimum inhibition control (pink), maximum inhibition control (blue) and a moxicillin dose response. DMSO <5% served as a minimum inhibition control, moxicillin 3X MIC value: 0.3mM was used as a maximum inhibitory control and moxicillin 0.6mM was used as the dose response reference control.

Upon reaching an OD_{600} of 0,6-0,8, bacteria were diluted to a starting OD_{600} of 0.001 of which 50µL of the diluted culture was added to each well in the plate, including the control wells. The final volume per well was 100µL. All plates were sealed in a secondary container and incubated at 37^0C with 5% CO_2 and humidification. After incubating for 24hrs, Alamar Blue reagent (Sigma-Aldrich, South Africa) was added to each well of the assay plate and re-incubated for 18hrs.

MIC$_{90}$ Determination

Relative fluorescence units (RFU) were measured using the SpecraMax i3x plate reader at 540-590nm (Bio-Tek). Data were analysed using Softmax® Pro 6 Software. The Software used a parameter curve fit protocol to calculate MIC$_{90}$. Raw RFU data were normalised to both the minimum and maximum inhibition controls to generate a dose response curve (% inhibition), using the Levenberg-Marquardt damped least squares method from which the MIC$_{90}$ was calculated. The lowest concentration of the drug that inhibits 90% of growth of the bacterial population is considered to be the MIC$_{90}$.

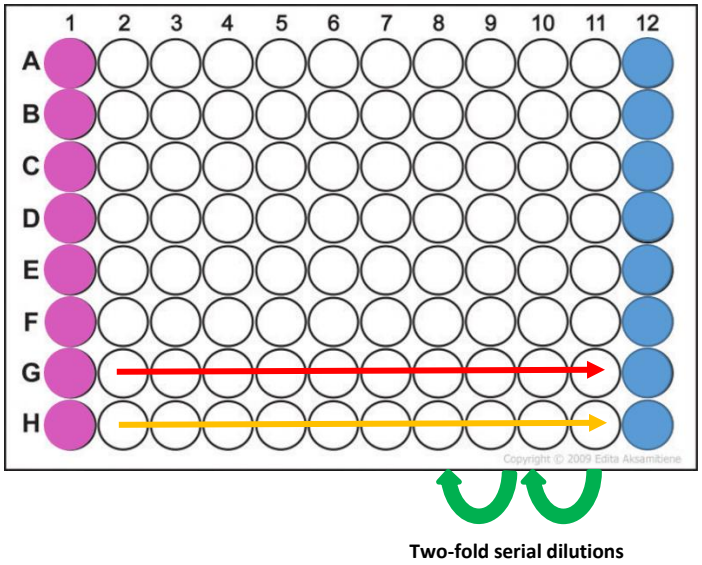

Figure 2. 4. **Alamar blue assay plate layout.**
Pink, minimum inhibition control in column 1 rows A-H. Blue, maximum inhibition control in column 12, rows A-H. Bold yellow arrow, dose response curve of reference drug column 2-11, rows A-H. Bold red arrow, media control, complete 7H9 Middlebrook media. Bold green arrows indicate start of serial dilutions from columns 11-2 in rows A-H. Adopted and modified from (57–59).

2.5 Growth conditions and analysis of survival in various stressors

Selected strains were grown (starting OD 0.001) in media containing various stressors that mimic macrophage intracellular conditions. OD$_{600}$ measurements were taken at different time points in each of the bacterial phase(s); Lag (OD$_{600}$ 0.001-0.4), Log/Exponential (OD$_{600}$ 0.5-0.8) and Stationary (OD$_{600}$ >1.00) (figure 10) using a

spectrophotometer (WPA, Whitehead Scientific). The data generated was analysed using GraphPad Prism 6. Culture samples were also taken for imaging by scanning electron microscopy (SEM).

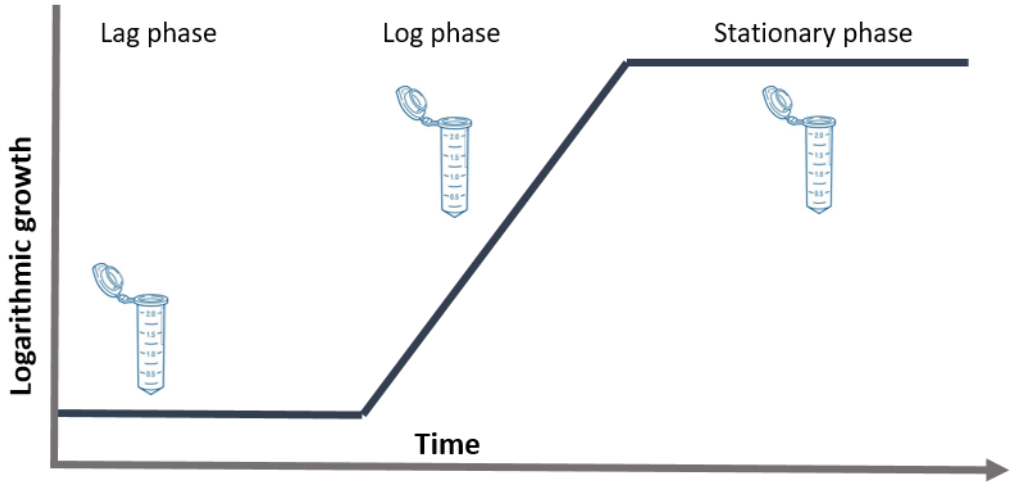

Figure 2. 5. **Plot showing phases of bacterial growth.**
Lag phase, a non-replicative period, Log phase, a replicative period and stationary phase presents cessation of replication. Cultures were collected in each growth phase in 2ml Eppendorf tubes for imaging by SEM. Adapted from (60).

Normal Complete 7H9 Middlebrook Media/ Normal Conditions

7H9 Media was prepared according to manufacturer's instructions. 2,3g of Middlebrook broth base (Sigma-Aldrich) was mixed with 450ml distilled water, 4ml glycerol and 1,25ml of 80% Tween (Merck). The media was sterilised by autoclaving at 121^0C for 10 min, left to cool to 45^0C and then supplemented with 10% Middlebrook Oleic Albumin Dextrose Catalase (OADC) (Becton Dickinson Biosciences, South Africa).

Osmotic Media/ Low Osmotic Stress

Osmotic media was made by depletion of NaCl. 10g Tryptone was mixed with 5g Yeast extract into 1L distilled water and autoclaved at 121^0C for 15min.

Nitrosative Media/ Stress Condition

1mM DETA-NO (Sigma-Aldrich) was added to 7H9 media to generate media containing nitric oxide radicals.

Antibiotic Media/ Stress

Rifampicin at a concentration of 1mM was added to complete 7H9 Middlebrook media.

2.6 Microscopy and Visualization

2.6.1 Scanning Electron Microscopy

Samples were prepared according to the SEM protocol of the Electron Microscope Unit at the Centre of Imaging (University of Cape Town, Division of Chemical Engineering, Upper Campus). Mutants were exposed to the different stressful media conditions and samples were taken at different time points as shown in figure 10. After centrifugation at 4000rpm for 30-60sec, samples were fixed with 2,5% (v/v) glutaraldehyde for approximately 8hrs in a 4^0C fridge. 1× PBS was used to rinse the samples before fixing with 1% (m/v) osmium tetroxide for approximately 1hr. Cells were spun and washed with 1× PBS and dH_2O to remove any excess osmium. Following a series of dehydrations in 30%, 50%, 70%, 90%, 95% and 100% ethanol, cells were re-suspended in 100% ethanol and mounted on microscope aluminium stubs. On the stubs, cells were dried by gently adding 2-3 droplets of Hexamethyldisilazane reagent (HMDS)(Sigma-Aldrich) and sputter coated with carbon. After 20min incubation at RT, samples were placed in the scanning electron microscope (SEM-MIRA) and images were recorded and analysed using the MIRA3 TESCAN programme.

2.6.2 Fluorescence Microscopy

Samples were prepared as previously described (61). Briefly, bacterial strains were cultured and incubated in stressful media conditions and then labelled with an analogue fluorescence dye, FM4-64(Invitrogen). Exponentially growing cells were washed 3 times with 1× PBS from the growth medium and re-suspended in 200µL 1× PBS containing 0,1µg/ml FM4-64 dye in ice cold Hanks Balanced Salt Solution (HBSS,

Sigma-Aldrich). Cells were incubated for 20-30min and a droplet of 1,5-2µL was mounted with Fluoromount before microscopic examination on the Zeiss Axioscope A1 Observer Inverted Microscope. Images were analysed using the ImageJ software.

Chapter 3: Results

Cloning and construction of *M. smegmatis* mutants

Chapter 3: Cloning and construction of *M. smegmatis* mutants

3.1 Amplification of *ftsE*, *ftsX*, *ftsEX* and *ripC* flanking regions from *M. smegmatis* genome

In order to investigate the role of *ftsE, ftsX, ftsEX* and *ripC* in *M. smegmatis*, upstream and downstream flanking regions of the genes were amplified from the genomic DNA of *M. smegmatis* MC^2155 using PCR. The upstream and downstream flanking regions of *ftsE* and *ftsX* were successfully amplified and observed as band sizes of 500bp as expected (figure 3.1, lanes 2-5). We also successfully amplified the *ripC* upstream flanking region that was observed as a 400bp band (figure 3.1, lane 6) and the downstream flanking region that was 300bp in size (figure 3.1, lane 7). We subsequently purified the PCR products using the Wizard® SV Gel and PCR Clean-up system (Promega) according to the manufacturer's instructions (Promega).

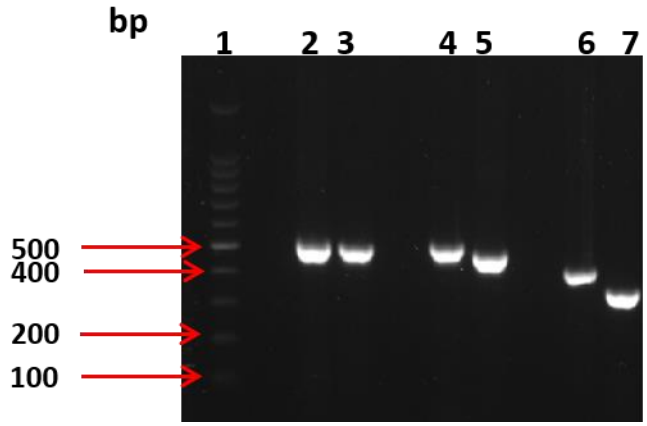

Figure 3. 1. **Generation of *ftsE, ftsX* and *ripC* upstream and downstream flanking regions.** PCR amplification was performed to amplify flanks of ±500bp.The PCR products were analysed on a 1% agarose gel and run for 1h at 100V using BIO-RAD Model 250/2,5 power system. Lane 1 is a 100bp DNA ladder, lanes 2-5 show bands at 500bp for upstream and downstream flanking regions of *ftsE* and *ftsX*. Lanes 6 and 7 is the upstream and downstream flanks for *ripC*.

3.1.1 Quantification of DNA with Nanodrop

We analysed the concentration and purity of the PCR products using a Nanodrop (Fluoroskan Ascent FL spectrophotometer). The *ftsE* upstream flank had a

concentration of 39.9ng/µl and a A260:280 ratio of 1.80 and the downstream flank had a concentration of 36.5ng/µl with a A260:280 ratio of 1.87. *ftsX* upstream and downstream flanking regions had a concentration of 37.7ng/µl and 35.7ng/µl with a A260:280 ratio of 1.86 and 1.80 respectively. The *ripC* upstream flank had a concentration of 37.8ng/µl and a A260:280 ratio of 1.80. The *ripC* downstream flank had a concentration of 36.9ng/µl with a A260:280 ratio of 1.98. All ratios were within the expected range, indicating that all DNA samples were pure.

Table 3. 1. **Quantification of 500bp flanking region DNA with Nanodrop**

M.smegmatis Flanking regions	ftsE	ftsX	ripC
Upstream DNA yield	36,9ng/µL	37,7ng/µL	37,8ng/µL
A260:280 ratio	1,80	1,86	1,80
Downstream DNA yield	36,5ng/µL	35,7ng/µL	36,9ng/µL
A260:280 ratio	1,87	1,80	1,98

3.2 Generation of 500bp-Hygromycin-500bp stitch product using overlap extension PCR

A PCR was performed to amplify HygR resistant cassette. The *HygR* gene was successfully amplified from a TOPO plasmid in which it was previously stored and was observed as a 1200bp band on agarose gel (figure 3.2, lanes 2 and 3). The PCR product was purified using the Wizard® SV Gel and PCR Clean-up system (Promega) according to the manufacturer's instructions (Promega). The HygR resistant cassette DNA had a high purity as indicated by the A260:280 ratio of 2.04 and 2.01 (table 3.2).

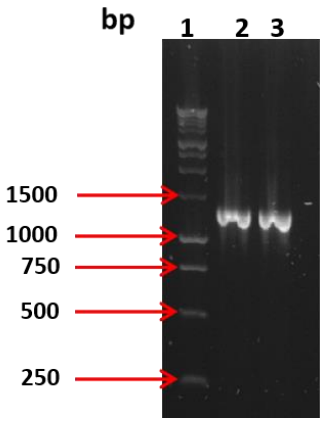

Figure 3. 2. **The Hygromycin resistance gene was successfully amplified by PCR.**
A PCR was performed to amplify HygR from a TOPO plasmid. Lane 1 is a 1kb ladder. Lanes 2 and 3 shows HygR product of 1200bp**.**

Table 3. 2. **Quantification of 1200bp Hygromycin resistance cassette DNA with Nanodrop**

HygR Sample	DNA yield	A260:280 ratio
Sample 1	325ng/µL	2,04
Sample 2	232ng/µL	2,01

The HygR cassette was subsequently stitched between the upstream and downstream flanking regions of each target gene as depicted in figure 2.1. We observed a stitch PCR product of approximately 2 200bp in lanes 2, 3, 4 and 5 corresponding to *ftsE*, *ftsX*, *ftsEX* and a *ripC* product of $^{+}/_{-}$ 2 000bp (figure 3.3, lane 5), demonstrating successful alignment between the flanking regions and the HygR cassette (figure 3.3, lanes 2-5). The faint band that was observed at 1200bp in lanes 2-4 is indicative of remnants of the HygR resistant cassette. The 2 200bp and $^{+}/_{-}$ 2 000bp stitch product was excised from the gel and purified using the Wizard® SV Gel and PCR Clean-up system (Promega) according to the manufacturer's instructions (Promega). The purified *ftsE* stitch product had a concentration of 63.3ng/µl and a A260:280 ratio of 1.98 (table 3.3). The *ftsX* stitch product had a concentration of 54.8ng/µl and a A260:280 ratio of 1.95. The stitch products for *ftsEX* and *ripC* had a concentration of 64.1ng/µl and 54.8ng/µl and A260:280 ratios of 2.00 and 1.95 respectively. (table 3.3).

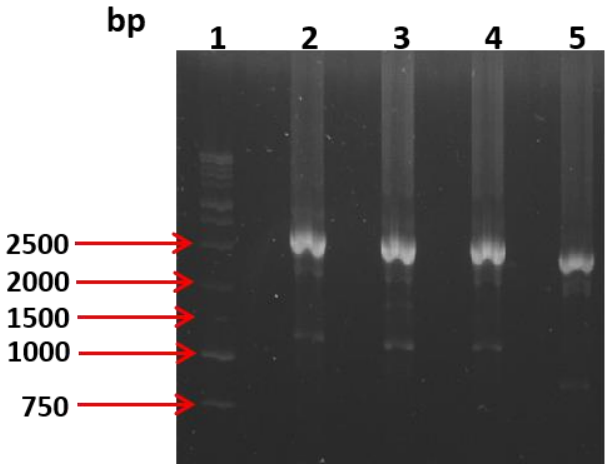

Figure 3. 3. **Screening of stitch products of 2200bp by Stitch PCR.**
HygR resistant cassette were stitched between upstream and downstream flanking regions. Lane 1 is a 1kb ladder. Lanes 2, 3 and 4 are the stitch products for ftsE, ftsX and ftsEX. Lane 5 is the stitch product for ripC.

Table 3. 3. **Quantification of 500bp-Hygromycin-500bp stitch products using a Nanodrop**

M.smegmatis Stitch product Samples	DNA Yield	A260:280 ratio
ftsE HygR	63,3ng/µL	1,98
ftsX HygR	54,8ng/µL	1,95
ftsEX HygR	64,1ng/µL	2,00
ripC HygR	54,8ng/µL	1,95

3.3 Transformation of MC²155 competent cells with pJV53 plasmid

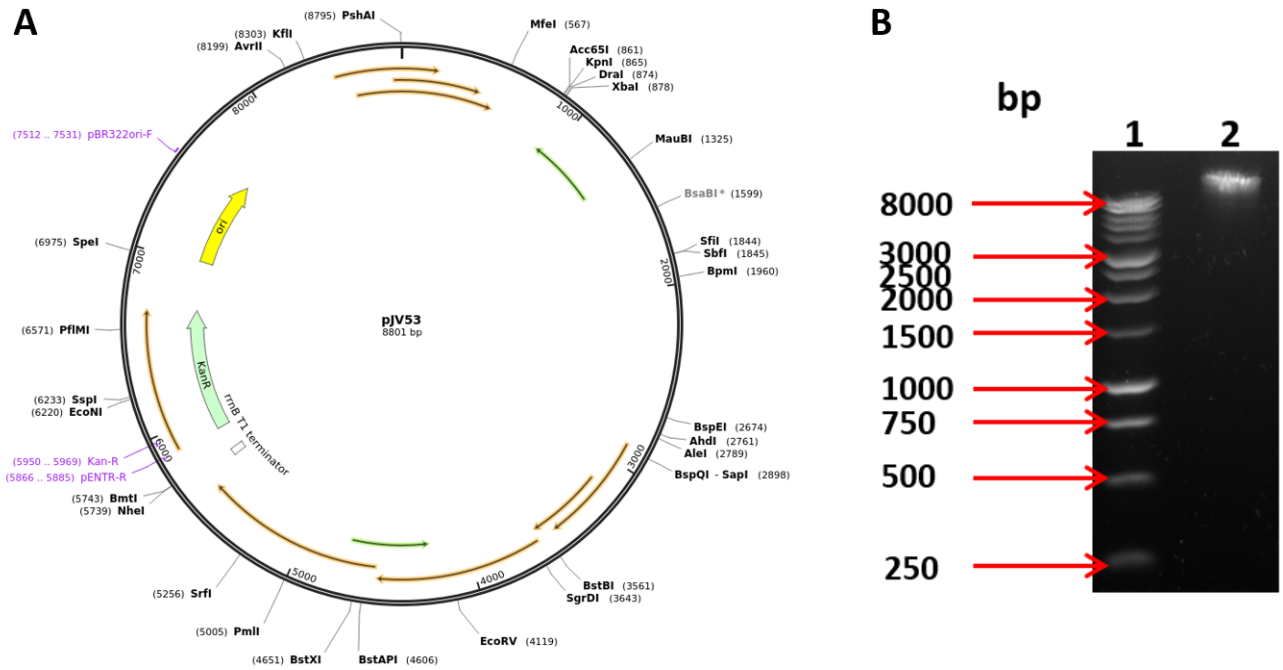

Figure 3. 4. **Successful isolation of pJV53 plasmid.**

Isolation of pjV53 recombineering plasmid from *E. coli* DH5-α cells. *M. smegmatis* cells were transformed with pJV53. (A) represents an image of pJV53 plasmid. (B) shows screening of pJV53 by agarose gel electrophoresis, lane 1, 1kb DNA ladder, lane 2, pJV53 plasmid DNA product.

pJV53 plasmid is widely used for gene recombination (62). *M. smegmatis* MC²155 cells were transformed with pJV53 into wildtype electro-competent cells and selected on 7H10 agar with 25µg/ml kanamycin. We successfully isolated pJV53 plasmid from *E. coli* DH5-α cells, which was indicated by the clear bright band above 8 000bp observed in lane 2 (figure,3.4B) As expected, no colonies were observed in the negative control, where no DNA was added during electroporation (figure 3.5A). Small circular colonies were seen indicating successful transformation of competent cells with pJV53 plasmid (figure 3.5B).

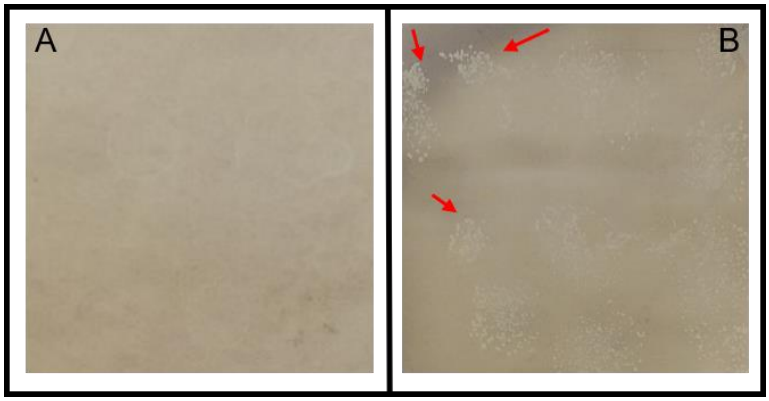

Figure 3. 5. **Transformation of MC²155 competent cells with pJV53.**
M. smegmatis cells were transformed with pJV53. (A) is the negative control (no DNA added) and (B) shows transformed sample. Red bold arrows show colonies selected on 7H10 agar supplemented with kanamycin (25µg/mL).

3.3.1 Deletion of *ftsE*, *ftsX*, *ftsEX* and *ripC*

Next, we generated mutant strains in which the genomic copies of *M. smegmatis ftsE*, *ftsX*, *ftsEX* and *ripC* were replaced with a hygromycin resistance cassette. The stitch PCR products for the respective target genes was electroporated into *M. smegmatis* that was previously transformed with pJV53 plasmid using the Lonza Nucleofector™ 2b high efficiency electro-transformation protocol. The bacteria was allowed to recover in 7H9 media for 2 hours and selected on 7H10 agar plates containing kanamycin. The transformation was successful as we obtained colonies for all the mutants (figure 3.6A-E). We picked a single colony for each gene for further screening by colony PCR.

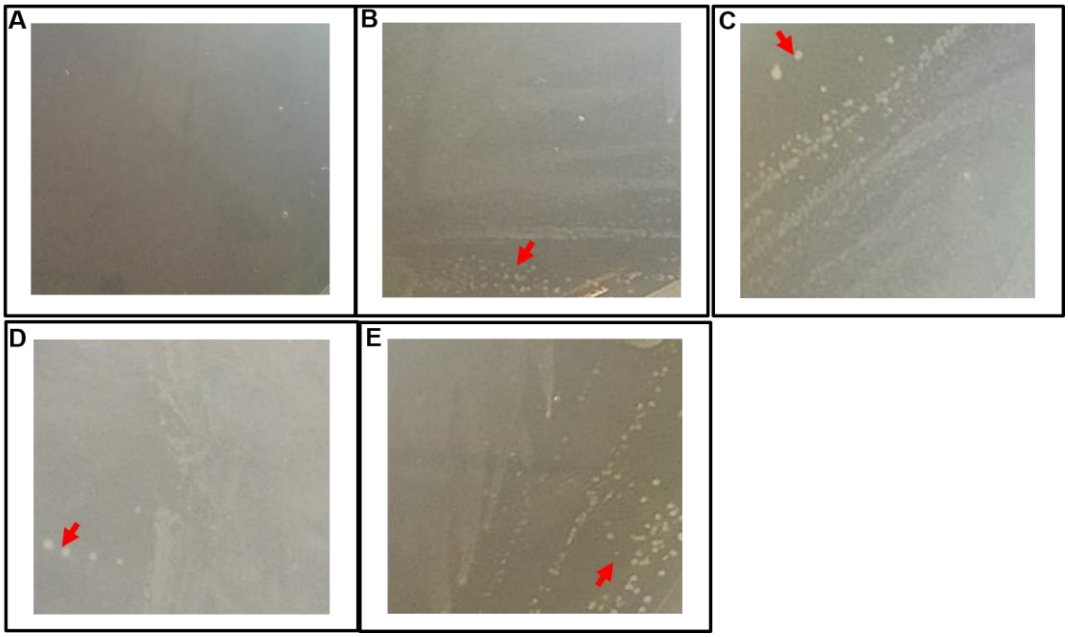

Figure 3. 6. **Transformation and selection of mutants on 7H10 agar.**
Selection of successfully electroporated mutant strains on 7H10 Middlebrook plates supplemented with 50µg/mL hygromycin and 25µg/mL kanamycin. (A) Control (no DNA was added during electroporation) (B)Δ*ftsE*, (C) Δ*ftsX*, (D) Δ*ftsEX* and (E) Δ*ripC.*

We selected single colonies and confirmed successful gene deletion by checking for the presence of the hygromycin resistance cassette of 1200bp using the MJ156 and MJ157 primers. We successfully amplified a 1200bp product for all the mutants confirming successful recombination of stitch product into the genome of *M. smegmatis* (figure 3.7A-D). We screened four colonies per gene denoted S1-S4 and all contained the 1200bp HygR cassette (figure 3.7). The positive control (purified HygR PCR product) was successfully amplified and observed as a 1200bp product as expected (figure 3.7A-D, lane 2). Therefore, we successfully generated *ftsE* (figure 3.7A), *ftsX* (figure 3.7B), *ftsEX* (figure 3.7C) and *ripC* (figure 3.7D) mutant *M. smegmatis*.

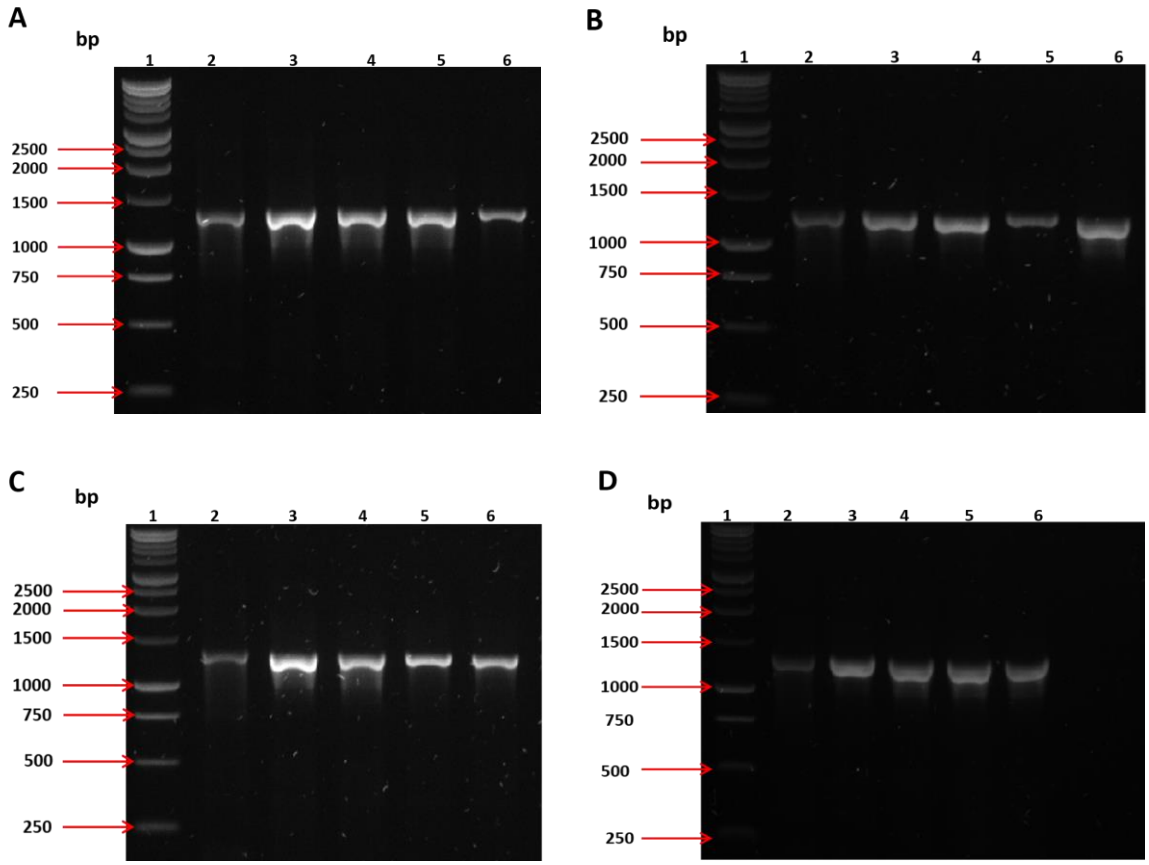

Figure 3. 7. **Analysis of colony PCR by gel electrophoresis.**

Selected clones were screened for the presence of hygromycin resistance cassette using primers MJ156 and MJ157. L represents 1kb DNA ladder, (+ve) is the positive control using purified HygR DNA as template and S1-S4 indicate one colony per target gene (4 replicates). (A) Δ*ftsE*, (B) Δ*ftsX*, (C) Δ*ftsEX*, (D) Δ*ripC.*

Chapter 4:
Characterization of survival patterns of *M. smegmatis* ftsEX and ripC mutants in various stressful conditions

Chapter 4: Characterization of survival patterns of M. smegmatis ftsEX and ripC mutants in various stressful conditions

4.1 MIC Determination

4.1.1 *ftsEX* and *ripC* deletion results in altered sensitivity to chloramphenicol

To determine antibiotic susceptibility of the mutants, we performed MIC_{90} assays using three of the first line TB drugs; rifampicin, isoniazid, ethambutol and a broad-spectrum antibiotic, chloramphenicol. The visual MIC_{90} is defined as the lowest concentration of drug that prevents a colour change. Blue coloured wells represent samples that had 90% inhibition, hence no bacterial growth, while pink coloured wells represent those that had growth. Relative fluorescence units (RFU) analysis for rifampicin drug (figure 4.1A) indicated that WT *M. smegmatis* MC^2155 had an MIC_{90} that ranged between 0.5-0.3mM (figure 4.1A & B). Although Δ*ftsE*, Δ*ftsX,* Δ*ftsEX* and Δ*ripC* were sensitive to rifampicin, the strains unexpectedly required a slightly higher drug concentration and had an MIC_{90} that ranged between 1.2-0.6mM (figure 4.1A-F).

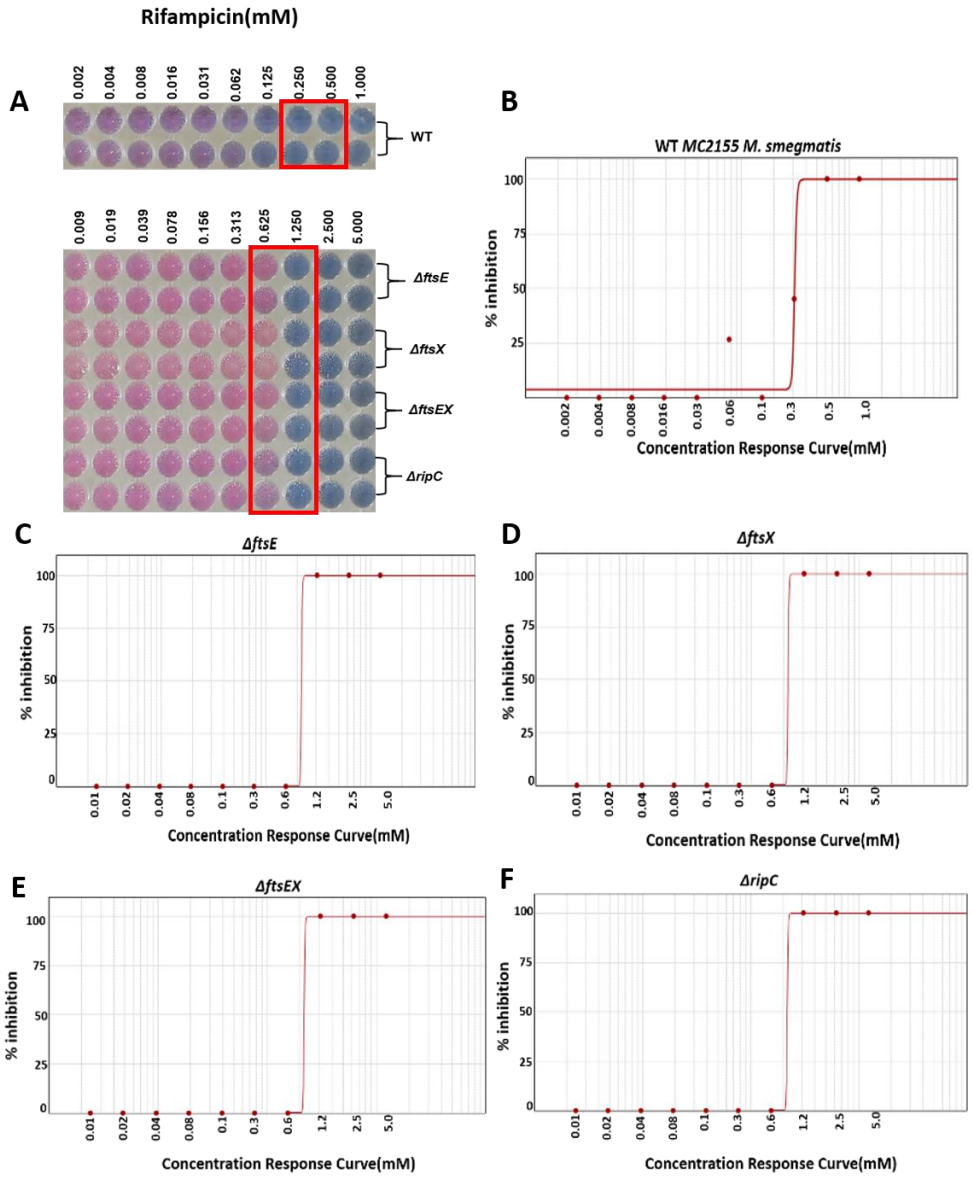

Figure 4. 1. **Rifampicin MIC plate analysis.**

Alamar blue MIC determination assay against rifampicin drug after 42-hour incubation. (A) Visual image of Alamar blue MIC determination assay for rifampicin. Dose response curves represent the percentage inhibition/calculated MIC_{90} against (B) WT *M. smegmatis MC²155*, (C) *ΔftsE*, (D) *ΔftsX*, (E) *ΔftsEX*, (F) *ΔripC*. MIC_{90}/Relative fluorescence units (RFU) readouts were measured using the SpecraMax i3x plate reader and analysed using Softmax® Pro 6 Software. The experiment is a representation of three independent experiments. For each experiment, samples were tested in duplicates. The drug concentration range for WT *M smegmatis MC²155* is 1.0-0.002Mm, and 5.0-0.01mM for all mutant strains.

The MIC_{90} for chloramphenicol for the WT was between 2.5-1.2mM (figure 4.2A & B). Compared to the WT, *ΔftsE* and *ΔripC* showed increased susceptibility to chloramphenicol with a much lower MIC_{90} (0.3-0.1mM, figure 4.2C & F). *ΔftsX* had the

same MIC_{90} for chloramphenicol as when it was treated with rifampicin, which ranged between 1.2-0.6mM (figure 4.2D). *ΔftsEX* was less sensitive to chloramphenicol with an MIC_{90} of 2.5-1.2mM (figure 4.2E).

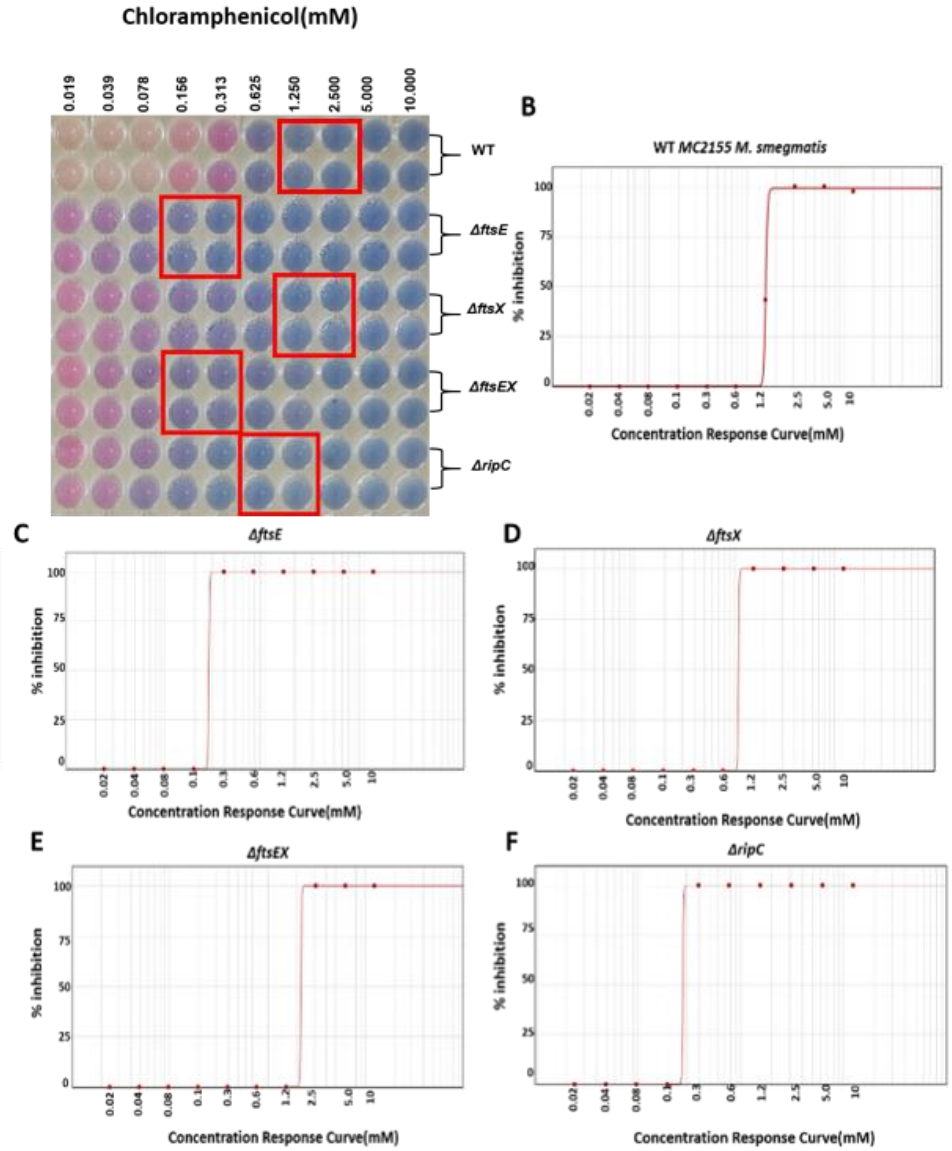

Figure 4. 2. **Chloramphenicol MIC plate analysis. Alamar blue MIC determination assay for chloramphenicol drug after 42-hour incubation.** (A) Visual image of Alamar blue MIC determination assay for chloramphenicol. Dose response curves represent the percentage inhibition/calculated MIC_{90} against (B) WT *M. smegmatis MC²155*, (C) *ΔftsE*, (D) *ΔftsX*, (E) *ΔftsEX*, (F) *ΔripC*. MIC_{90}/Relative fluorescence units (RFU) readouts were measured using the SpecraMax i3x plate reader and analysed using Softmax® Pro 6 Software. Samples were tested in duplicates. The drug concentration range for all strains is 10-0.02mM.

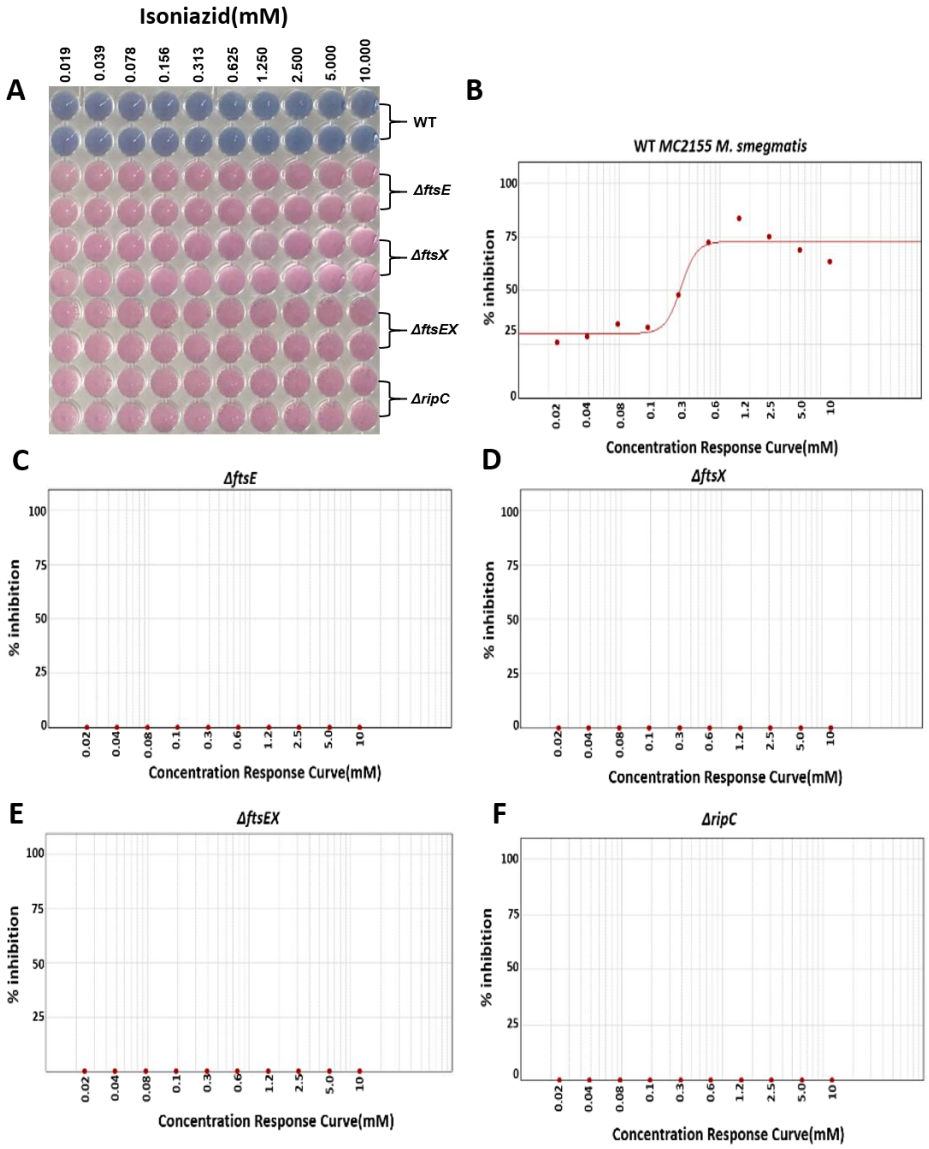

Figure 4. 3. **Isoniazid MIC plate analysis.**

Alamar blue MIC determination assay against isoniazid drug following 42-hour incubation. (A) Visual image of Alamar blue MIC determination assay for isoniazid drug. Dose response curves present the percentage inhibition/calculated MIC_{90} against (B) WT *M. smegmatis MC²155*, (C) *ΔftsE*, (D) *ΔftsX*, (E) *ΔftsEX*, (F) *ΔripC* mutants. MIC_{90}/Relative fluorescence units (RFU) readouts was measured using the SpecraMax i3x plate reader and analysed using Softmax® Pro 6 Software. The drug concentration range for WT. *smegmatis MC²155* and for all mutant strains is 10-0.02mM.

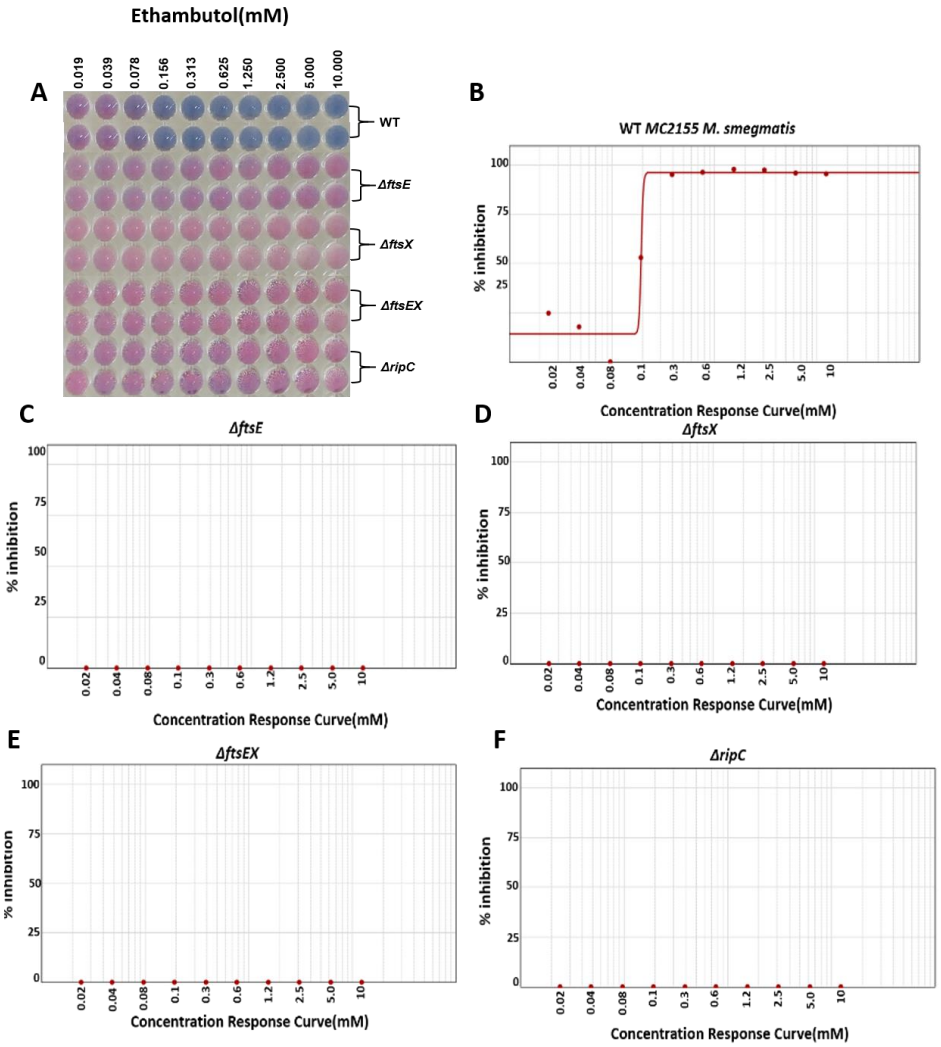

Figure 4. 4. **Ethambutol MIC plate analysis.**

Alamar blue MIC determination assay for ethambutol drug after 42-hour incubation period. (A) Visual image of Alamar blue MIC determination assay for ethambutol drug. Dose response curves represent the percentage inhibition/calculated MIC_{90} against (B) WT *M. smegmatis MC²155*, (C) ***ΔftsE***, (D) ***ΔftsX***, (E) ***ΔftsEX***, (F) ***ΔripC*** mutants. MIC_{90}/Relative fluorescence units (RFU) readouts was measured using the SpecraMax i3x plate reader and analysed using Softmax® Pro 6 Software. Samples were tested in duplicates. The drug concentration range for WT. *smegmatis MC²155* and for all mutant strains is 10-0.02mM.

4.2 Growth Curves

4.2.1 *ftsEX and ripC* are required for *M. smegmatis* survival in various stressors

Genes that govern normal division and elongation are likely to be essential for bacterial survival. Based on this, we wanted to investigate whether the loss of *ftsEX* and *ripC* will compromise the ability of *M. smegmatis* to grow normally under *in vitro* stressful conditions that mimic host immune responses. In normal conditions, all the mutants grew at a similar rate as the WT bacteria and displayed similar growth dynamics from lag into exponential phase (figure 4.5A). However, when grown in salt depleted LB broth (low osmotic media), the mutant strains grew poorly reaching a peak OD_{600} of 0.25-0.30 after 40hrs whereas the WT bacteria grew normally under these conditions (figure 4.5B). Therefore, these data demonstrated that *ftsE*, *ftsX*, *ftsEX* and *ripC* are required for bacterial growth in low osmotic conditions.

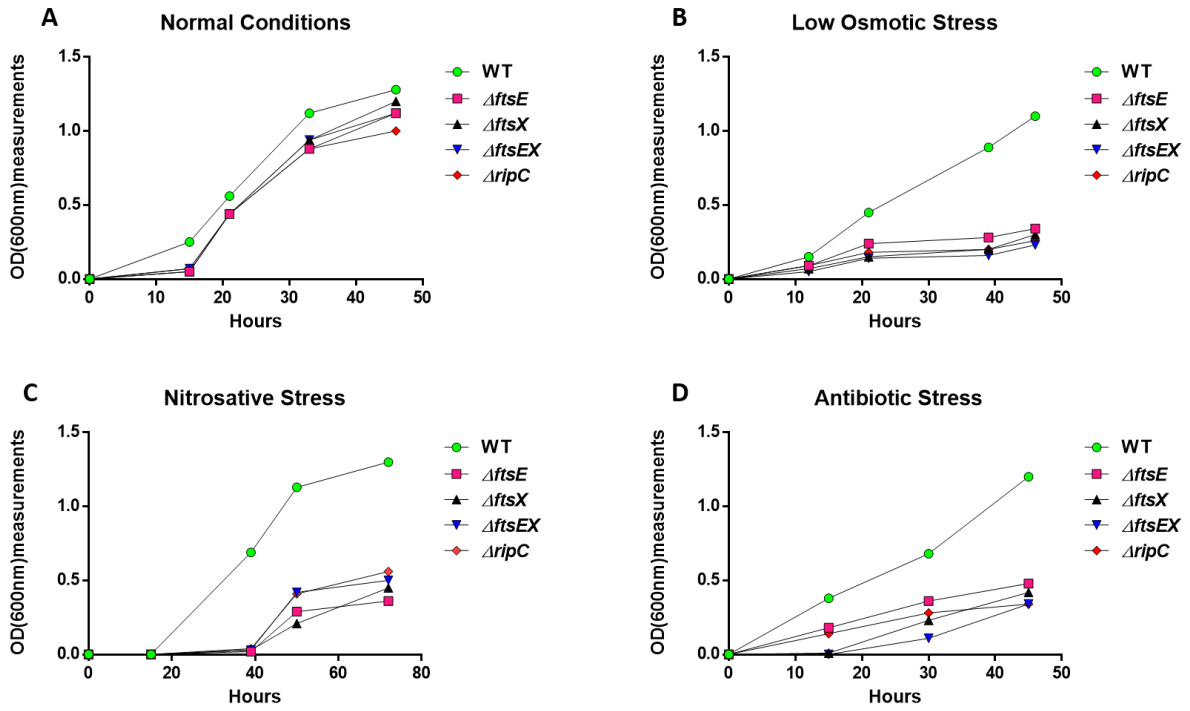

Figure 4. 5. **Survival of WT and KO strains when subjected to *in vitro* stressful conditions.** Growth curves of WT MC²155 *M. smegmatis*, Δ*ftsE*, Δ*ftsX*, Δ*ftsEX* and Δ*ripC*. Survival of *M. smegmatis* WT *MC²155,* Δ*ftsE*, Δ*ftsX*, Δ*ftsEX* and Δ*ripC* in (A) normal 7H9 media, (B) low osmotic media, (C) 7H9 media containing 1.0mM diethylenetriamine nitric oxide (DETA-NO) and (D) 7H9 media containing

1.0mM rifampicin drug. The data is a representation of 3 experiments. All strains were grown in duplicates.

ΔftsEX and *ripC* growth and survival was also investigated by exposure to nitrosative stress using a slow release nitric oxide donor called DETA-NO. WT exhibited a delayed growth of 18hrs in this condition and then resumed normal growth dynamics (figure 4.5C). However, all the mutants struggled to grow in media containing DETA-NO as displayed by their temporary cessation of growth for 40hrs and subsequent poor growth rate with a short exponential phase and maximal OD_{600} of around 0.5 (figure 4.5C). Finally, we exposed WT, *ΔftsEX* and *ripC* to rifampicin after determining concentrations using MIC assay (figure 4.1). OD_{600} measurements showed that both *ΔftsX* and *ΔftsEX* struggled to grow relative to *ΔftsE* and *ΔripC* (figure 4.5D). Though *ΔftsX* and *ΔftsEX* suffered into an exponential phase, a small population of persister cells still managed to escape and fight the stress reaching an OD_{600} of 0.4 after 46hrs (figure 4.5D). Overall, these results suggested that *ΔftsEX* and *ΔripC* may be sensitive to treatment with rifampicin.

Chapter 5: Results
Cell elongation and division specific characterization

Chapter 5: Cell elongation and division specific characterization

5.1 Microscopy

5.1.1 *ftsEX* and *ripC* are not essential for growth in normal conditions

To characterize growth-related phenotypes of *ftsEX* and *ripC mutants* in various stressful conditions, growth phase dependent imaging was performed using scanning electron microscopy (SEM). Under normal conditions, all the mutants exhibited a similar morphology to WT *M. smegmatis* cells in all the growth phases except for *ΔftsX* mutants that displayed a filamentous or an unusually short length at the log and stationary phases on growth (figure 5.1). *ΔftsX* filaments had a size of 20.0μM compared to that of the WT with an average cell length of *2*.4μM (figure 5.5, see appendix).

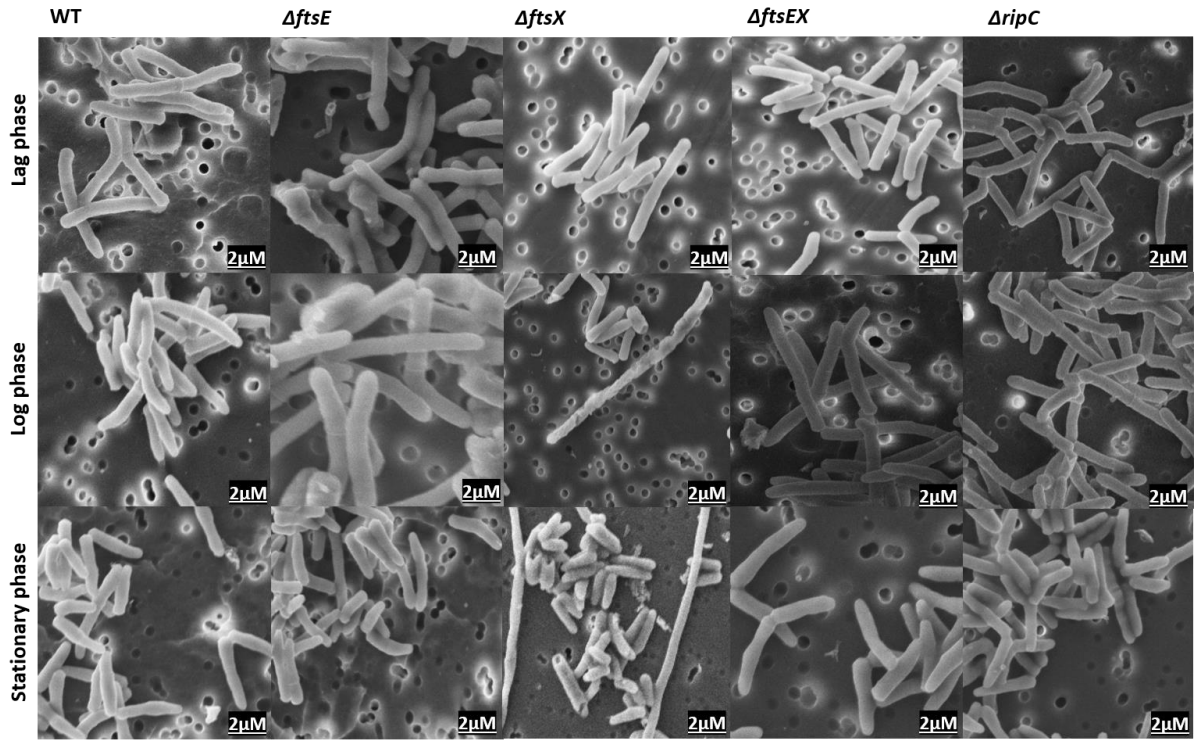

Figure 5. 1. **Growth analysis of *M. smegmatis* under normal conditions by scanning electron microscopy.** 48-hour analysis of WT *MC²155 M. smegmatis*, Δ*ftsE, ΔftsX, ΔftsEX* and *ΔripC* under normal conditions. WT viewed at 20X magnification in lag, log and exponential phase. Δ*ftsE*, 20X magnification in lag, log and exponential phase. *ΔftsX* 20X magnification in lag, log and stationary

phase. *ΔftsEX,* 20X magnification in lag, log and stationary phase. *ΔripC,* 20X magnification in lag, log and exponential phase. All strains were grown in duplicates. Scale bar = 2µM.

5.1.2 *ftsEX* and *ripC* deletion results in growth defects in low osmotic stress

Significant morphological changes were seen between the WT and mutant strains when cells were under low osmotic stress (figure 5.2). No phenotypic difference was seen for the WT cells (figure 5.2). In contrast, visible differences in cell length and morphology were seen in *ΔftsE*, *ΔftsX*, *ΔftsEX* and *ΔripC* mutants. All mutants had a combination of short and long cells which were seen in lag, log and stationary phase (figure 5.2). Cells that were shorter in length were bulgy while those that were longer in length had a filamentous phenotype (figure 5.2). Furthermore, the septum for some of the filamentous cells appeared to be invaginate which was accompanied with visible chaining (figure 5.2). Another important observation is the extreme bulging which was exclusively observed for *ΔftsEX* in stationary phase (figure 5.2).

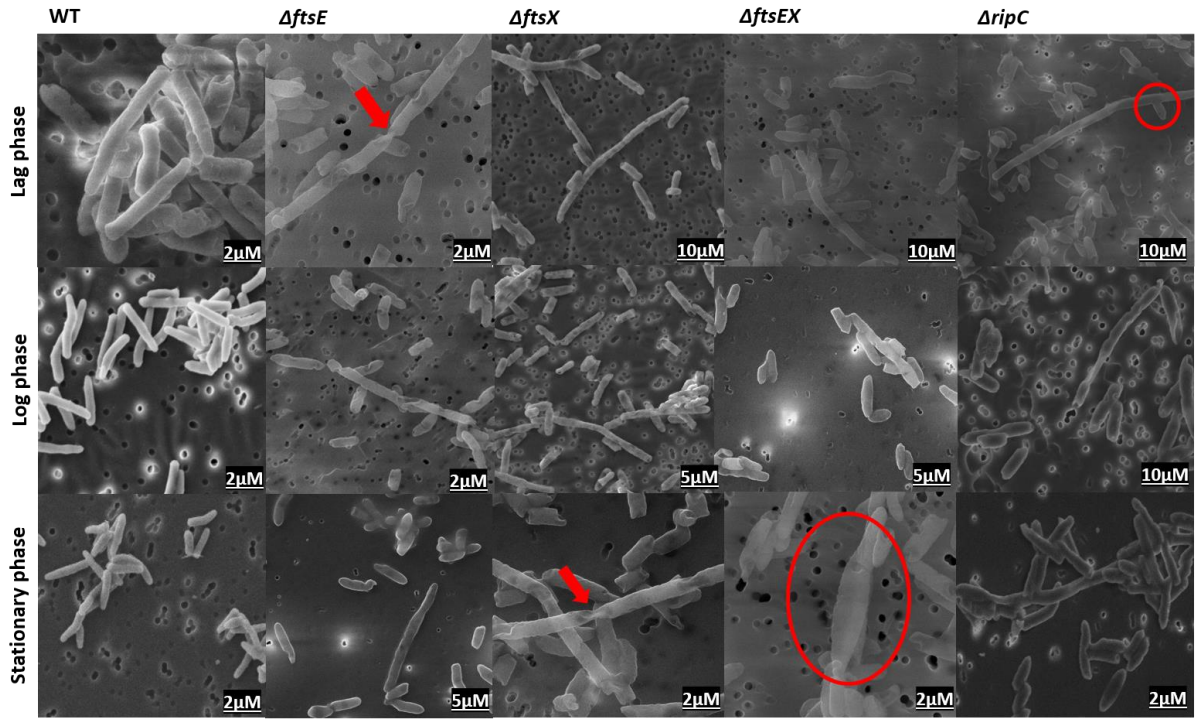

Figure 5. 2. **Scanning electron microscopy of *M. smegmatis* cells in low osmotic media condition.** 48-hour analysis of WT *MC²155 M. smegmatis*, Δ*ftsE, ΔftsX, ΔftsEX* and *ΔripC* in low osmotic media conditions. Salt depleted LB broth was used to create low osmotic stress. WT 20X magnification in lag, log and exponential phase. Δ*ftsE*, 20X magnification in lag and log phase and 5X in exponential phase. *ΔftsX* ,10X magnification in lag phase, 5X in log phase and 20X in stationary phase. *ΔftsEX* ,10X magnification in lag phase, 5X in log phase and 20X in stationary phase. *ΔripC,* 10X magnification in

lag and log phase and 20X in exponential phase. Bold red arrows indicate chaining and red bold oval shaped circles shows bulging. Strains were grown in duplicates. scale bar ranges =2 and 10µM.

5.1.3 *ftsEX* and *ripC* deletion produce a chaining phenotype during nitrosative stress

We observed no abnormalities in the WT strain when it was exposed to the nitrosative stress (figure 5.3). All four mutants displayed morphological defects which included cell chaining, branching and bulging (figure 5.3). Branching was observed for *ΔftsE* and occurred near the cell pole during lag and log phase, which was similar to those observed in stationary phase for *ΔftsX*. With respect to cell length, a heterogenous population of cells were visible when *ΔftsEX* and *ΔripC* mutants entered the log phase, while it was only observed when *ΔftsE* and *ΔftsX* entered stationary phase (figure 5.3). Two prominent observations were made for *ΔftsEX,* in log phase, bulging occurred along the cell periphery while in stationary phase, the filamentous cell abnormally expanded outwards near the poles (figure 5.3). Deletion of *ΔripC* produced a chaining phenotype during log phase (figure 5.3). *ΔripC* cells were also extremely short and stumpy in comparison to WT (figure 5.3).

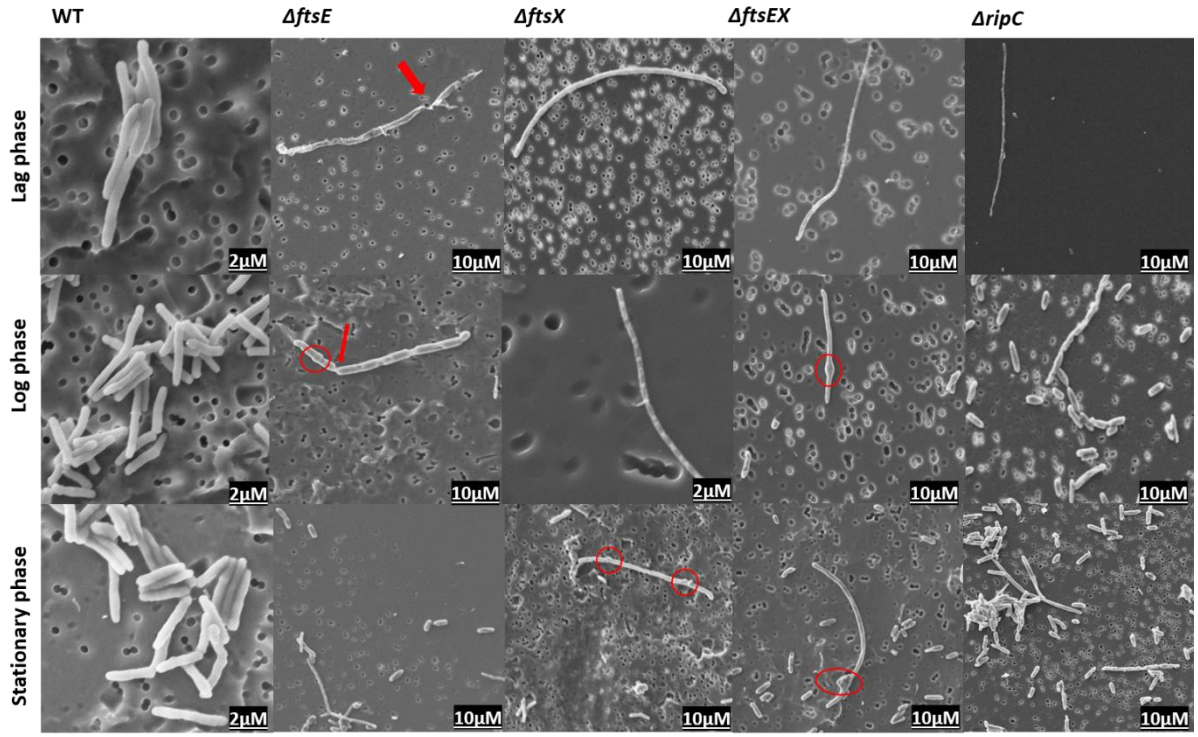

Figure 5. 3. **Growth analysis of *M. smegmatis* by scanning electron microscopy.**

72-hour analysis of WT *MC²155 M. smegmatis*, Δ*ftsE, ΔftsX, ΔftsEX* and *ΔripC* under nitrosative stressful conditions. The concentration of DETA-NO was 1mM. WT, 20X magnification in lag, log and exponential phase. Δ*ftsE,* 10X magnification in lag, log and exponential phase. *ΔftsX* ,10X magnification in lag phase, 20X in log phase and 10X in stationary phase. *ΔftsEX* ,10X magnification in lag, log and stationary phase. *ΔripC,* 10X magnification in lag, log and exponential phase. Bold red arrows indicate snapping, small bold circles show protruded ridges and bold oval shaped circles signify bulging. All strains were grown in duplicates. Scale bar ranges 2 and 10µM.

5.1.4 Mutant cells failed to maintain their shape during rifampicin treatment

The majority of the short cells for *ΔftsE* and *ΔftsX* had holes in their cell walls when they were exposed to rifampicin which was observed for one or two *ΔftsEX* cells (figure 5.4). WT cells lacked this characteristic and appeared to be unaffected by the exposure to rifampicin (figure 5.4). In stationary phase, no filamentation was observed in Δ*ftsE, ΔftsX, ΔftsEX* and Δ*ripC* cells (figure 5.4). Along with the altered cell lengths (figure 5.13, appendix) , the short cells in *ΔftsE*, *ΔftsX ΔftsEX* and Δ*ripC* looked fatter and bulgier (figure 5.4). *ΔftsX* however, had a distinct filamentous cell that was partially curved with unusual branching along the pole of the cell (figure 5.4).

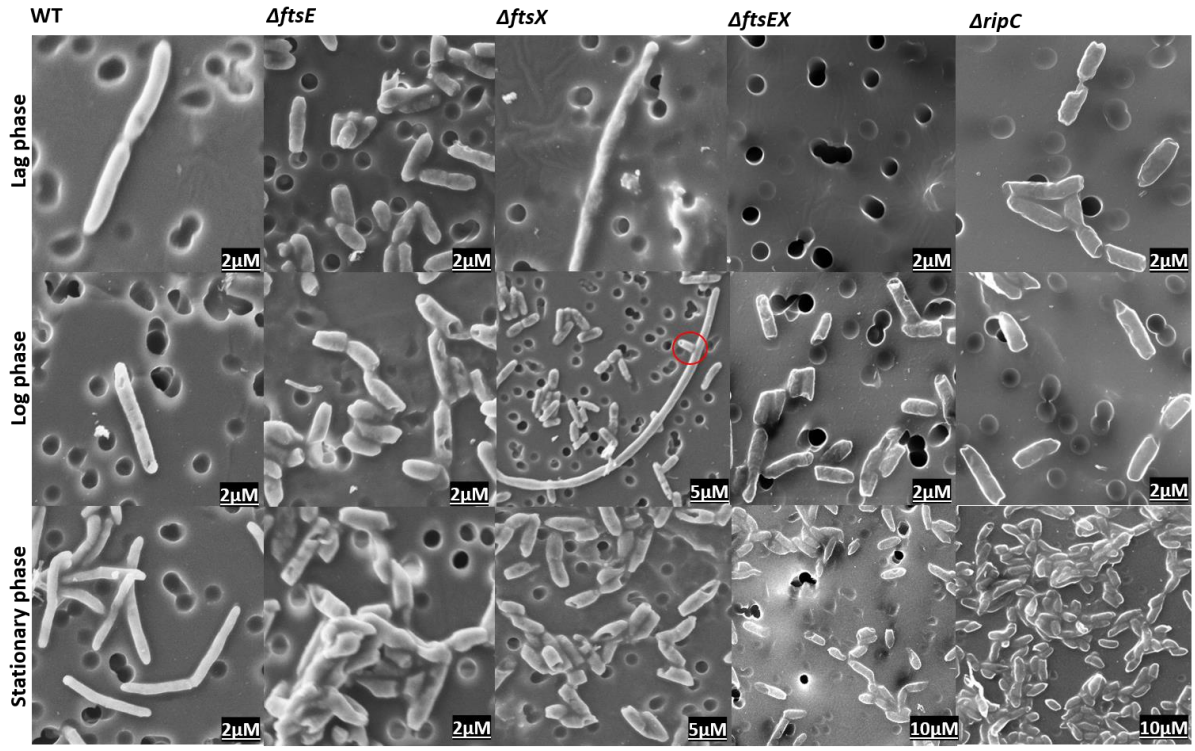

Figure 5. 4. **Growth curve analysis of *M. smegmatis* by scanning electron microscopy.**

48-hour analysis of WT *MC²155 M. smegmatis*, Δ*ftsE, ΔftsX, ΔftsEX* and *ΔripC* under antibiotic stress. Concentration of rifampicin drug was 1mM. WT viewed at 20X magnification in lag, log and exponential phase. Δ*ftsE* ,20X magnification in lag, log and exponential phase. *ΔftsX* ,20X magnification in lag and 5X in log and stationary phase. *ΔftsEX* ,20X magnification in lag and log and 10X in stationary phase. *ΔripC,* 10X magnification in lag, log and exponential phase. Bold small circle shows unusual branching. Strains were grown in duplicates. Scale bar ranges =2,5 and 10µM.

Chapter 6: Discussion

Chapter 6: Discussion

Cell division is a fundamental process in the life cycle of all bacteria (63). The entire process must be carefully co-ordinated and requires tight regulation in response to environmental changes (3). Bacterial proliferation is divided into two main processes; elongation and division (11). Large multiprotein complexes known as the elongation complex and divisome help maintain a constant balance between cell wall degradation and synthesis. When a bacterial cell divides, it enlarges its peptidoglycan layer and subsequently divides it too (64). Hence PG remodelling is important for bacterial growth and depends on the modulating activities of these complexes.

PG hydrolases play a key role in coordinating the breakdown of PG. The exact time and space are important for this coordination because it enables faithful sharing of the cell wall material to facilitate daughter cell separation. In our study, we focused on a cell wall protein complex FtsEX and periplasmic PG hydrolase, RipC. Homologs of FtsEX exist in distantly related bacterial species and consistent trends of evidence link it to a key role in regulation of PG hydrolysis during elongation and division. Little is known about FtsEX and RipC in growth and division, particularly of its role in the context of immune related stressors. Hence, we investigated the biological essentiality of *M. smegmatis* FtsEX and RipC in stressful conditions that mimic the immune related conditions and antibiotic stress *in vitro*.

We successfully generated FtsEX and RipC mutant strains by knocking out the gene of interest using a 2200bp product that contained the upstream and downstream flanking regions stitched to a HygR cassette. We then determined sensitivity of *ΔftsEX* and *ΔripC* to anti-TB drugs using Alamar blue MIC determination assays. We found that mutants were more sensitive to chloramphenicol (figure 4.2 and 5.10, appendix) but not to rifampicin (figure 4.1 and 5.9, appendix), isoniazid (figure 4.3) and ethambutol (figure 4.4). Both isoniazid and ethambutol had pink wells indicating growth and were thus excluded from the analysis (figure 5.11 -12, appendix). Unlike rifampicin, small agents like chloramphenicol gain periplasmic access by using porin proteins which could account for the increase in sensitivity seen against the drug (65). Though more sensitivity was observed against chloramphenicol, we found that the MIC_{90} of *ΔftsEX* and *ΔripC* was corresponding to that in the literature (3).

Subsequently we selected rifampicin as an antibiotic condition to be examined in our growth curve conditions.

Bacteria employ different strategies to survive when they encounter unfavourable environmental conditions (66). We evaluated the growth dynamics of the mutants in media lacking essential minerals or supplemented with harmful molecules to mimic the harsh environment the bacteria encounter inside a macrophage. All the mutants and wild-type bacteria exhibited similar growth dynamics in normal 7H9 media, suggesting that Δ*ftsE,* Δ*ftsX,* Δ*ftsEX* and Δ*ripC* are not essential for survival in normal conditions. Conversely, growth was severely altered in the absence of salt/salt depleted media which is similar to what was observed for *ΔftsEX* in *E. coli* (54). Bacterial growth is stimulated when solute accumulation occurs in a high osmotic environment (67). As a result, an osmotic stress response where bacteria are deprived of essential salts alters the growth rate. Moreover, cellular growth and expansion is highly dependent on the ability of bacterial cells to maintain the cell's turgor pressure which is also regulated by osmoregulatory processes (67,68). Deleting cell wall specific genes confer a structural change which has also been shown to be directly proportional to indirect osmosensing (69). In this case, FtsEX and RipC might also be involved in osmosensory and regulatory processes because changes in the solvent concentration in both the periplasmic and cytoplasmic spaces may be detected by membrane based osmosensors when cell wall changes occur (67–69).

Additionally, mutants were almost completely disarmed under nitrosative stressful conditions, suggesting that they struggled to cope with the toxic effects that were induced by the nitric oxide releasing agent. DETA-NO has a half-life of $^{+}/_{-}$18 hours, hence our WT resumed growth likely because the NO in the media had been exhausted. Even when under what has been described as considerably low nitrosative stress in the literature, mutants appeared to be extremely sensitive for an additional 22 hrs before viability was slowly restored after a short but rapid growth period (figure 4.5C) (70). Moreover, there is a reduction in NO radical generation, hence the mutant population manages to grow to a peak OD of 0.6. This could simply be that the bacteria have adapted over time, however, a higher dose might have extended or effectively inhibited growth over a longer time frame.

Previous work has shown that several genes were upregulated during Mtb infection of activated macrophages when under mid-range concentrations of NO (0.5-5mM) (71). Although standard laboratory protocols were used to recreate nitrosative stress, these findings also indicate that the concentration of DETA-NO used in our experiment are most likely comparable to what is experienced by a bacterial cell within a macrophage environment.

Previous work by Rego et al.,2017 studied the relationship between cell wall integrity and antibiotics and found that cells depleted of LamA, a member of the divisome, are rapidly killed by rifampicin and other drugs targeting the cell wall. These findings therefore suggested that deletion of mycobacterial divisome factors are associated with rifampicin sensitivity. Hence, we investigated the susceptibility of FtsEX and RipC in response to treatment with the drug. In our antibiotic growth curve analysis, we found that rifampicin was able to retard/restrict the growth of all the mutant strains. Mavrici and colleagues showed that sublethal concentrations of rifampicin severely inhibit the growth of *ΔftsEX* and *ΔripC* mutants (3). Rifampicin is known to inhibit transcription by targeting RNA polymerase (rpoB) (72). On that account, hypersensitivity of the mutants to rifampicin could be due to the need for efficient transcription of a functionally redundant system (3). The sensitivity of the mutants could also mean that drugs are accumulating at higher levels than the WT due to changes in the cell wall (3).

Depletion of FtsEX generates cell shape defects characterized by filamentous cells that are completely assembled but not separated (51). We decided to do growth phase dependent imaging, to look for cell division specific characteristics such as defects in elongation and/or division. Consistent with their non-essential role in normal conditions, the FtsE, FtsEX and RipC mutants had similar morphological phenotypes with the WT strain. The deletion of FtsX, however, resulted in the formation of a heterogeneous population comprising of shorter or lengthier cells in normal conditions. Although the changes were minor, the results suggest that FtsX might possibly be required for cell elongation/division in normal conditions. Since FtsE directly interacts with FtsX, we had expected the deletion of FtsE to phenocopy the same cell defects caused by deletion of FtsX, however, this was not the case, particularly in normal conditions. This finding contrasts with that observed for FtsE and FtsX in *S. pneumoniae* (73). Interestingly, the resulting cell division defects were not correlated

with a reduced growth rate in normal 7H9 media. This can be partially attributed to the idea of uncoupled cellular elongation and division during the growth cycle of mycobacteria. Since the division cycle is governed by time and not cell size/shape, such a defect may not have a direct inhibitory effect on the division and elongation process (74). On this note, the continued growth (figure 4.5A) seen for *ΔftsX* in the absence of normal elongation and division are consistent with the depletion of cell division components such as hydrolases in several other bacterial species. For instance, in *E. coli*, neither single nor double mutations in any of the three amidases, AmiA, B and C, affected the growth rate (75). Nevertheless, these observations make us question how normal growth continues to occur when cells form chains or when they fail to elongate properly.

Most mutations in various cell division genes are osmoremedial (55). This led to the notion that the division process itself might intrinsically be sensitive to low osmotic strength (54). Supporting evidence has also shown that interrupting amidase activity and disrupting interaction with FtsX under low osmolarity resulted in the formation of filamented cells (55). The same effect was seen for *ΔftsE, ΔftsX, ΔftsEX* and *ΔripC*, in addition to the other phenotypes that included bulging, visible chaining and cell membrane invagination. The type of unusual bulging phenotype displayed by *ΔftsEX* could be due to failure in cell pole maturation (76). Nevertheless, most of the cells are shorter and bulgy in this condition, indicative of possible defects in elongation. The low proportion of mutant cells that were in the form of filaments had membrane invaginations, indicating that there might be a significant stall in division. This led to our assumption that FtsEX might have a possible role in facilitating proper septum cleavage. Moreover, cells tend to form long chains when PG hydrolases are not activated, so they continue to elongate without cell division which is evident in our findings (3,77).

We also noted that the extremely lengthy filament in RipC mutant contained what appears to look like a short “arm” along its length. This type of branching has previously been reported by Senzani et al.,2017 who investigated the role of an amidase called Ami1 in *M. smegmatis* (78). Single cell time lapse microscopy showed that a growth determining component called DivIVA, is responsible for pole determination in *M. smegmatis*. DivIVA is important because it drives the elongation machinery to continue even if division is stalled or if a block in septum cleavage occurs

eventually resulting in the formation of lateral growth(s) and/or bud(s). Growth in the chains of Ami1 mutants was associated with “ectopic mis-localisation” of DivIVA, which eventually resulted in the formation of lateral buds at a non-septal region, which was seen in *ΔripC* (79). Like *ΔAmi1,* the lack of RipC mostly resulted in short cells that failed to elongate. Nevertheless, these cells did not form lateral buds. RipC, like other amidases and/or hydrolases plays an important role to enable normal elongation in low osmotic stress.

Our results also contradict the finding by Rojas et al., 2014 who reported on the fundamental biomechanical and biochemical processes driving cell wall expansion and eventually cell growth (80). They reasoned that cell wall expansion and growth is not dependent on changes in osmotic pressure (80). In contrast, our mutants failed to survive and are required for normal elongation and division in conditions of low osmolarity (52). We are not certain whether osmotic pressure plays a key role in peptidoglycan insertion and ultimately growth and separation of daughter cells. It is mostly likely possible, because our understanding is that FtsE activates FtsX, which in turn activates predicted hydrolases and/or amidases that cleave bonds in the PG layer for insertion of newly synthesized material (3,53,73). In conclusion, the phenotypes in the salt depleted media may have resulted from cell wall changes caused by membrane leakiness that may have conferred osmotic sensitivity.

Loss of FtsEX and RipC produced two striking characteristics during exposure to nitrosative stress. The first was the extremely lengthy cells that were seen in all mutants during lag and log phase. *ΔripC*, however, had a proportion of short cells that were visible during log phase, which was only seen in stationary phase for *ΔftsE*, *ΔftsX* and *ΔftsEX*. The second characteristic(s) was that *ΔftsX* and *ΔftsEX* had formation of lateral branches that were distort out of shape, but, occurred near the cell poles, none of which was observed in the WT strain. Moreover, *ΔftsEX* cells also started bulging in log phase, as shown in figure 5.3. Previous studies in *S. pneumoniae*, showed that both environmental and antibiotic stresses have an impact on the catalytic enzymes involved in cell wall synthesis. Such predicaments cause cell wall deficiency and make the wall thinner eventually resulting in bulging and cell lysis (81). As an alternative of cell bulging, elongated cells can also form, which in this condition, were considerably thinner than usual. The reasoning might be hypothetical, but it could be feasible

because organisms become thin-walled when PG degradation occurs due to cell wall deficiency as a coping strategy for stress (81).

The concept behind mimicking macrophage induced nitrosative stress was to see whether either one of our target genes would play a significant role when engulfed by these phagocytes. Filamentation is required for virulence, exclusively because phagocytes struggle to engulf bacteria when in this form (82). This strategy may favour escape from phagocytosis but it is also limited (83). This phenotype is partially attributed to the so-called SOS response, a pathway that senses DNA damage. In *Salmonella enterica* serovar *typhimurium*, filamentation is initiated when inside macrophages as a result of nitro-oxidative stress which is driven by the SOS response (82). Additionally, exposure of *M. tuberculosis* to DNA damaging radicals *in vitro* and exposure to intracellular stress inside macrophages *in vivo* has also been associated with filamentation (82,84). When exponential cultures of *M. tuberculosis* were exposed to nitric oxide or nitric oxide related intermediates such as DETA-NO, an overall increase in cell length was seen (84). Mechanisms employed to prevent such cell division blockages and SOS-induced filamentation remain unknown (84). However, our findings reiterate the need for FtsEX and RipC for survival specifically in "macrophage like conditions". Interestingly, Mtb RipC has been shown to be required for virulence in a mouse model of TB infection (85).

In addition to their requirement against immune-like mediated stresses, our results showed that FtsEX and RipC seem to be conditionally essential in relation to antibiotic stress. WT cells were undamaged and intact, but majority of the mutants had holes in their walls. There is a slight similarity between these defects and "open holes", described as craters, when cells of *S. aureus* were exposed to antimicrobial peptides at sub and supra MIC's in salt free media (86). The holes could be as a result of membrane rupture, which can be due to loss of cell wall integrity (87). This observation supported the hypothesis that interrupting PG synthesis can cause an activation of autolytic cell wall enzymes, which can lead to autolysis, therefore the walls seem to be catastrophically compromised (88). It could also mean that deletion of FtsEX and RipC caused breaches in the cell wall, hence, the cells were unable to tolerate it. Another striking observation was the localization of these holes. We noted that they were found to be localized near the poles, which was also observed as "dented spots" in *B. subtilis* after treatment with chlorhexidine (89). The same damaged trait appeared

all over cells of *E. coli*, however, the localized morphological damages may be a division scar appearing next to the new pole after completion of a septum and daughter cell separation (90,91).

As previously reported for another mycobacterial hydrolase RipA, RipC also controls the degradative activities that are regulated through cell wall “protein-protein” interactions (43). If RipA requires careful control for growth and division, and is lethal when dysregulated, it is possible to expect the same when cells are deleted of RipC. This defect is pronounced since our results showed that both FtsEX and RipC function in the same pathway. Upon reaching stationary phase, mutants lost not only their shape, but also their ability to elongate. Mutant cells became fatter and swollen, implying that rifampicin exacerbated the already compromised defects in cells that were depleted of FtsE, FtsX, FtsEX and RipC.

Bacterial populations are thought to continue growth and division even when exposed to antibiotic concentrations where majority of the cells are killed. For example, Zhu et el., 2018 describes it as “antibiotic tolerance” but proposed that it encompasses a spectrum of phenotypes (72). In our study we found that deletion of FtsEX and/or RipC resulted in sensitivity to the drug which was also accompanied with an altered growth rate. Although cells were struggling to survive, a sub-population continued to grow which could be due to “tolerance”. Our microscopy results show an overall population of short bacterial cells with ruptured cell walls during rifampicin exposure, however, in their study, although considered a low dose, a higher dose was used, and cells started swelling 6 hours post antibiotic exposure. The unexpected phenotype could be due to the differences in antibiotic doses, exposure(time) but it could also be due to the essentiality of the genes indicating a potential role of FtsEX and RipC in maintaining wall integrity.

Cell division in mycobacteria can be challenging, particularly because of the complex mechanisms that bacteria regulate to meet them (40). To accommodate growth processes which include elongation, division and differentiation, continuous remodelling, degradation, and cell wall synthesis must occur. What is important between all these processes is the integrity of the cell wall. Lack of hydrolytic activity is known to have a “domino effect” on the structural changes in the PG layer (92). It implies that a loss in “PG editing enzymes” would lead to repercussions in structural

changes and cell wall integrity. We further investigated whether loss of FtsEX and RipC will compromise cell wall integrity during normal and low osmotic conditions using fluorescence microscopy. As expected, loss of FtsE, FtsX, FtsEX and RipC did not have any effect on the membrane integrity under normal conditions (figure 5.5, appendix). Like the WT strain, all mutant membranes were intact and had evenly distributed fluorescence patterns.

In *Agrobacterium tumefaciens* cells stained with FM4-64 dye, both old pole and new pole membranes were equally labelled, but the septal sites were not. This type of "horseshoe" staining pattern was not observed in our results. Furthermore, cells about to divide also had no staining at the construction site, which is consistent with what has been shown by Zupan et al., 2013. It was noted that the entire endomembrane of *Arabidopsis thaliana* stained with FM4-64, and was due to impaired plasma membrane integrity (93). The given examples may have demonstrated different patterns of FM4-64 staining; however, our results show that precision in mid-cell division is clear because cells are actively dividing. This is apparent by the uniform fluorescence pattern observed in the membranes of WT and mutant strains. These findings reiterate our conclusion that deletion of FtsEX and RipC did not jeopardize the integrity of the wall in normal conditions.

Membrane integrity was extremely compromised under low osmotic stress (figure 5.6). Although cells were clumping, which is as a result of the stress condition, clear membrane disintegration is seen amongst *ΔftsE*, *ΔftsX*, *ΔftsEX* and *ΔripC* cells. Cells fail to undergo normal elongation and division resulting in bulging and possible osmolysis which was observed by lysed/ruptured cells and cell fragments. These defects imply that lack of FtsEX and RipC impairs and obstructs the PG synthesis process eventually compromising cell wall integrity and morphology. In addition, concentrated sites of FM4-64 was observed in these conditions, which did not occur when cells were exposed to normal conditions. Cells depleted of MurG resulted in a similar bulging defect and when stained with FM4-64, had unclear patterns of staining and localisation (ref). In conclusion, Muchová et al., 2011 proposed it could be residual sites of PG synthesis occurring at sites of septation (94). The same reasoning could be applied in our study; however, no definite conclusions can be made until further investigation.

Concluding remarks

Our study reported on the cell wall complex, FtsEX and the periplasmic amidase, RipC, and their role in cell elongation and division in the context of immune-like stressful conditions and antibiotic stress. We showed that FtsEX and ripC mutants fail to survive when exposed to low osmolarity, nitrosative stress and rifampicin. Thus, FtsEX and RipC have been proven to be conditionally essential for survival in *M. smegmatis.* Deletion of FtsEX and/or RipC generates cell shape defects characterised by short cells, bulging, filamentation, lateral branching, membrane invagination and possible ectopic pole formation. Similarly, deletion of FtsEX or interacting partners and/or downstream signalling proteins yield division like defects in several other bacterial species (3,50,52,53). In conclusion, FtsEX and RipC are involved in key processes governing normal cell wall elongation and division to enable *M. smegmatis* survival of stress.

Future studies

In addition to cloning FtsE, FtsX and RipC in *M. smegmatis*, we also managed to amplify the upstream and downstream 500bp regions of *M. tuberculosis (*figure 5.8, appendix*)*. The intention was to characterize *M. tuberculosis* survival in macrophages and the mechanisms of the protective role played by FtsEX in intracellular stressful conditions. After several attempts of DNA recombination, we did not succeed in generating Mtb knockouts.

Our *M. smegmatis* FtsEX and RipC mutants were further analysed by MIC assays, growth curves and microscopy. In addition to the above-mentioned experiments that were performed, we also attempted transmission electron microscopy using protocols as described by (95–97). The problem we encountered here was the fixing of these cells, therefore, as an alternative, we proceeded with scanning electron microscopy.

The clumping of cells in low osmotic media conditions interfered with our imaging analysis in fluorescence microscopy, therefore we decided to exclude this from our results. Despite this hurdle, both scanning (figure 5.1-4) and fluorescence (figure 5.8, appendix) microscopy showed that loss of FtsEX and RipC resulted in the production of heterogenous phenotypes during stress. Though our results provide insights onto the FtsEX mechanism, it also indicates the need for further investigation. Hence, due to the limitations in the study, we proposed the following:

- To verify interaction between FtsE, FtsX and RipC using the bacterial two hybrid system analysis.
- To determine detailed mechanisms of FtsEX driven protection through complementation of FtsEX and RipC with a plasmid expressing the native genes.
- To further investigate the importance of Mtb FtsEX-RipC interaction on the protection of Mtb within host cells since the same amino acid residues present *in M. smegmatis* FtsX are also present in *M. tuberculosis.*

Appendix

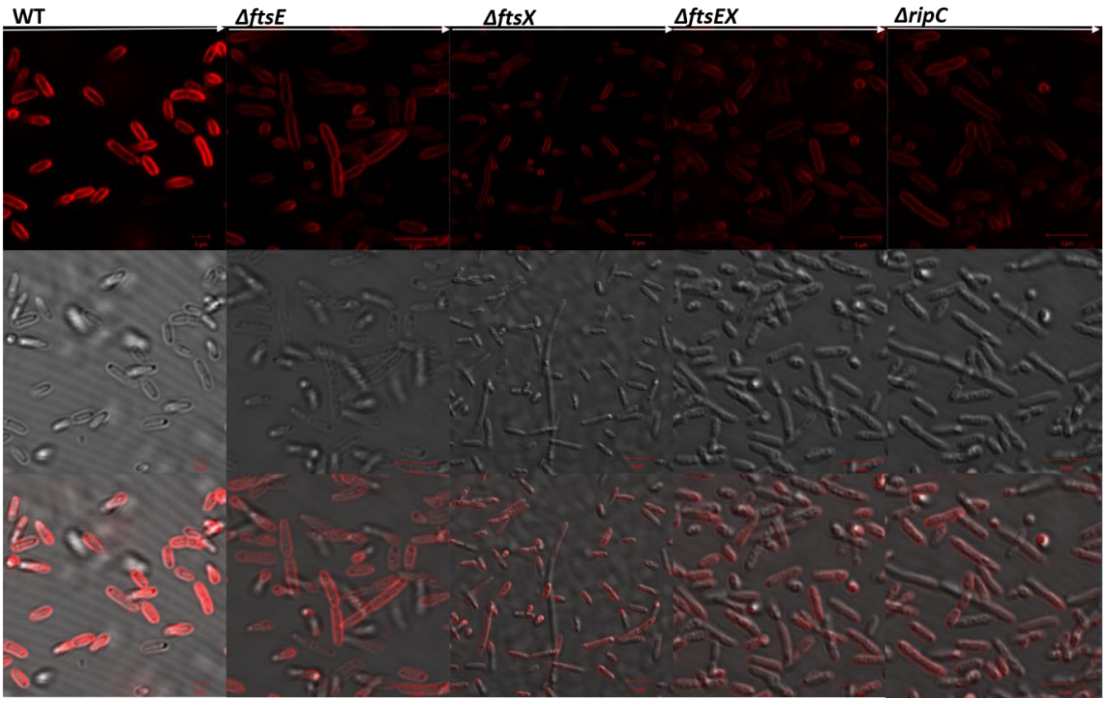

Figure 5. 5. **Visualization of FM4-64 membrane staining of *M.* smegmatis in normal 7H9 media by fluorescence microscopy.** *WT MC² 155 M. smegmatis, ΔftsE, ΔftsX, ΔftsEX, and ΔripC.* 0.1µg/ml FM4-64 used for staining. Scale bar 2-5µM.

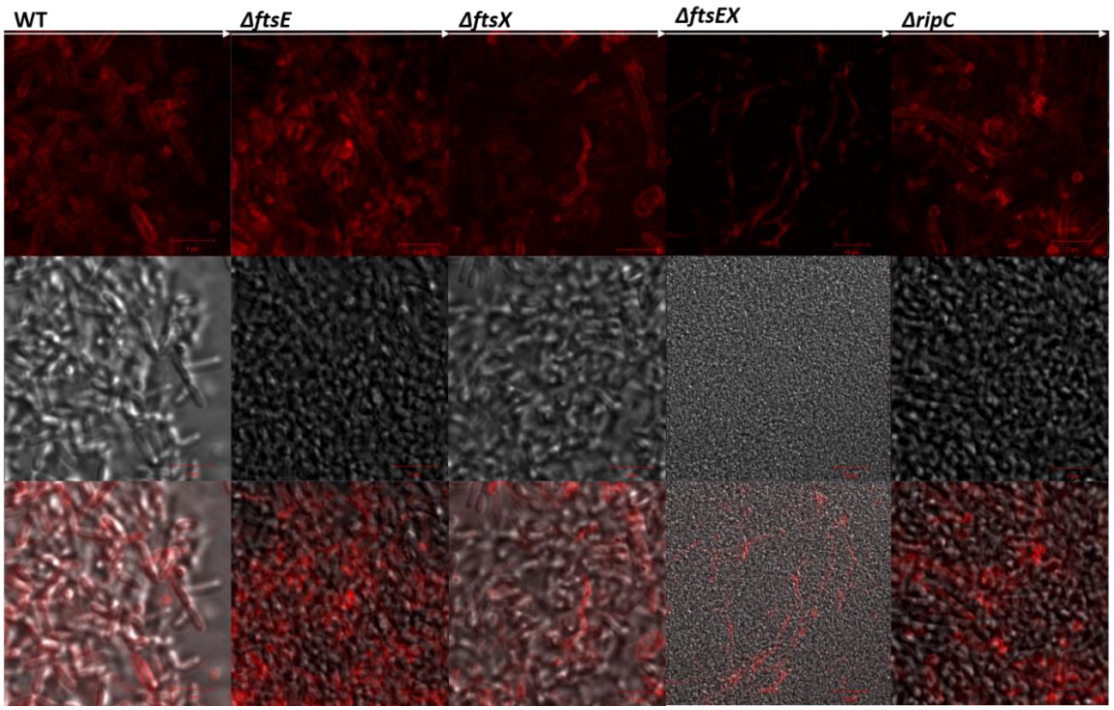

Figure 5. 6. **FM4-64 membrane staining of *M. smegmatis* in low osmotic media conditions by fluorescence microscopy.** WT *MC² 155 M. smegmatis*, Δ*ftsE*, *ΔftsX*, *ΔftsEX*, and *ΔripC*. 0.1µg/ml FM4-64 used for staining. Scale bar 5µM.

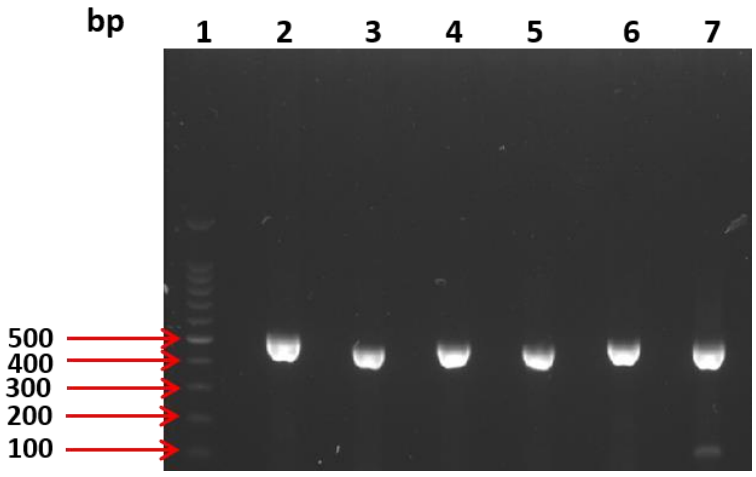

Figure 5. 7. **Generation of *FtsE, FtsX* and *RipC* upstream and downstream flanking regions *of M. tuberculosis* H37Rv.** Lane 1 is a 100bp DNA ladder, lanes 2 and 3, 500bp upstream and downstream flanking regions of *ftsE*, lanes 4 and 5, *ftsX*, lanes 6 and 7, *ripC*. Amplicons were visualized under UV by gel electrophoresis.

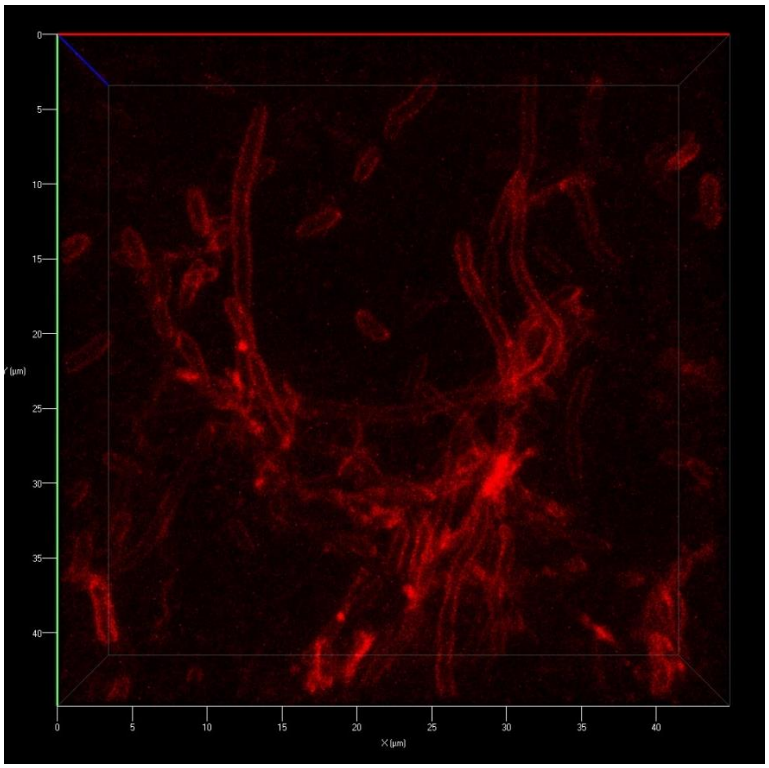

Figure 5. 8. **3D visualisation of FM4-64 membrane staining of *ΔftsEX* during low osmotic media conditions.** Loss of FtsEX produces heterogenetic phenotypes. 0.1µg/ml FM4-64 used for staining.

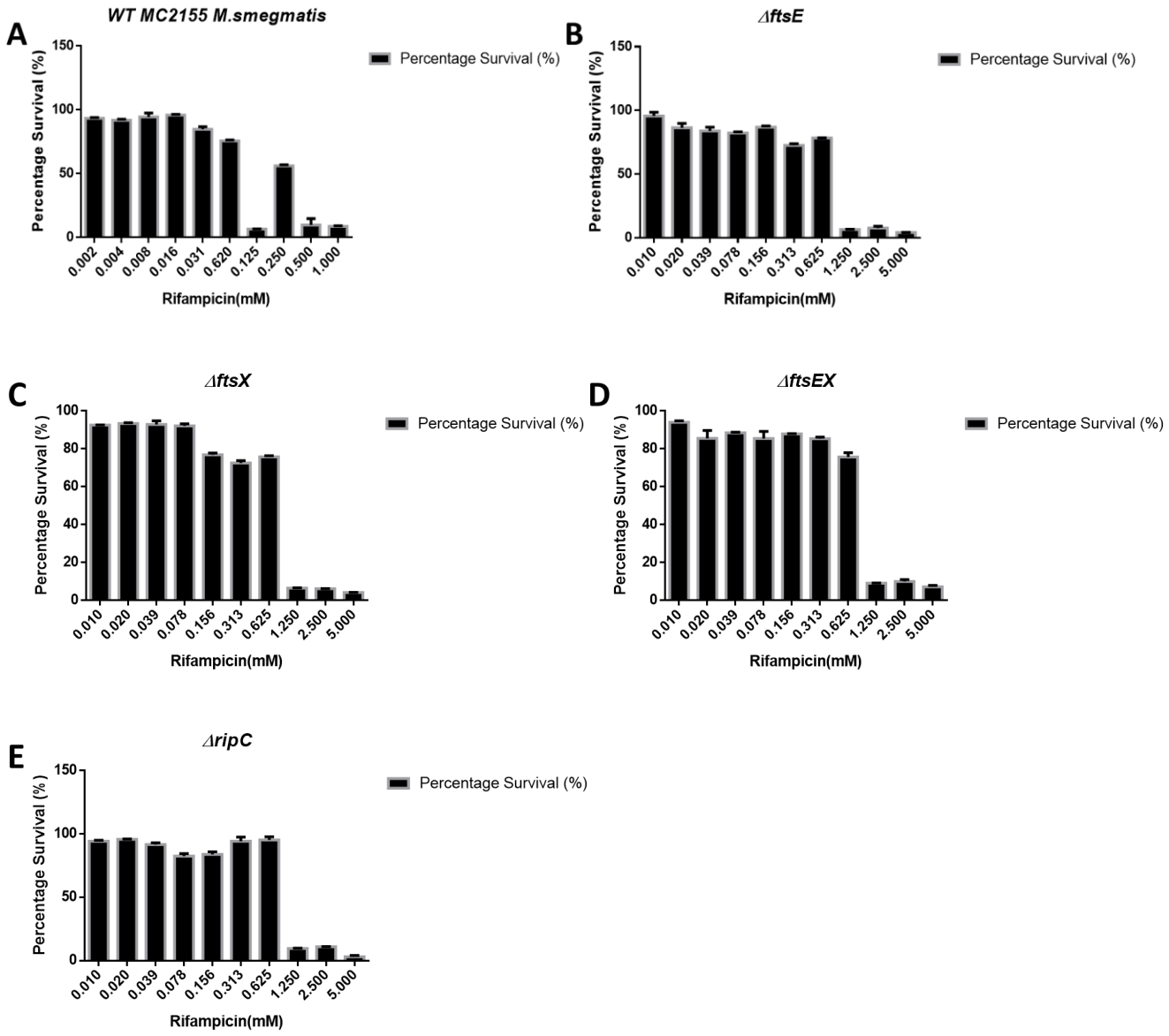

Figure 5. 9. **Percentage survival of *M. smegmatis* against rifampicin drug.** Each bar represents the relative fluorescence percentage (%) calculated from the RFU values determined by Alamar blue MIC assay against rifampicin drug. Percentage survival was determined for each strain at corresponding concentration (s). Raw RFU data were divided by the average of the cells only control and multiplied by 100 to get the percentage inhibition. Percentage survival were tallied by subtracting the percentage inhibition from 100. The error bars represent standard error of the mean (SEM) derived from duplicates. (A) WT *M. smegmatis MC²155*, (B) *ΔftsE*, (C) *ΔftsX*, (D) *ΔftsEX*, (E) *ΔripC*.

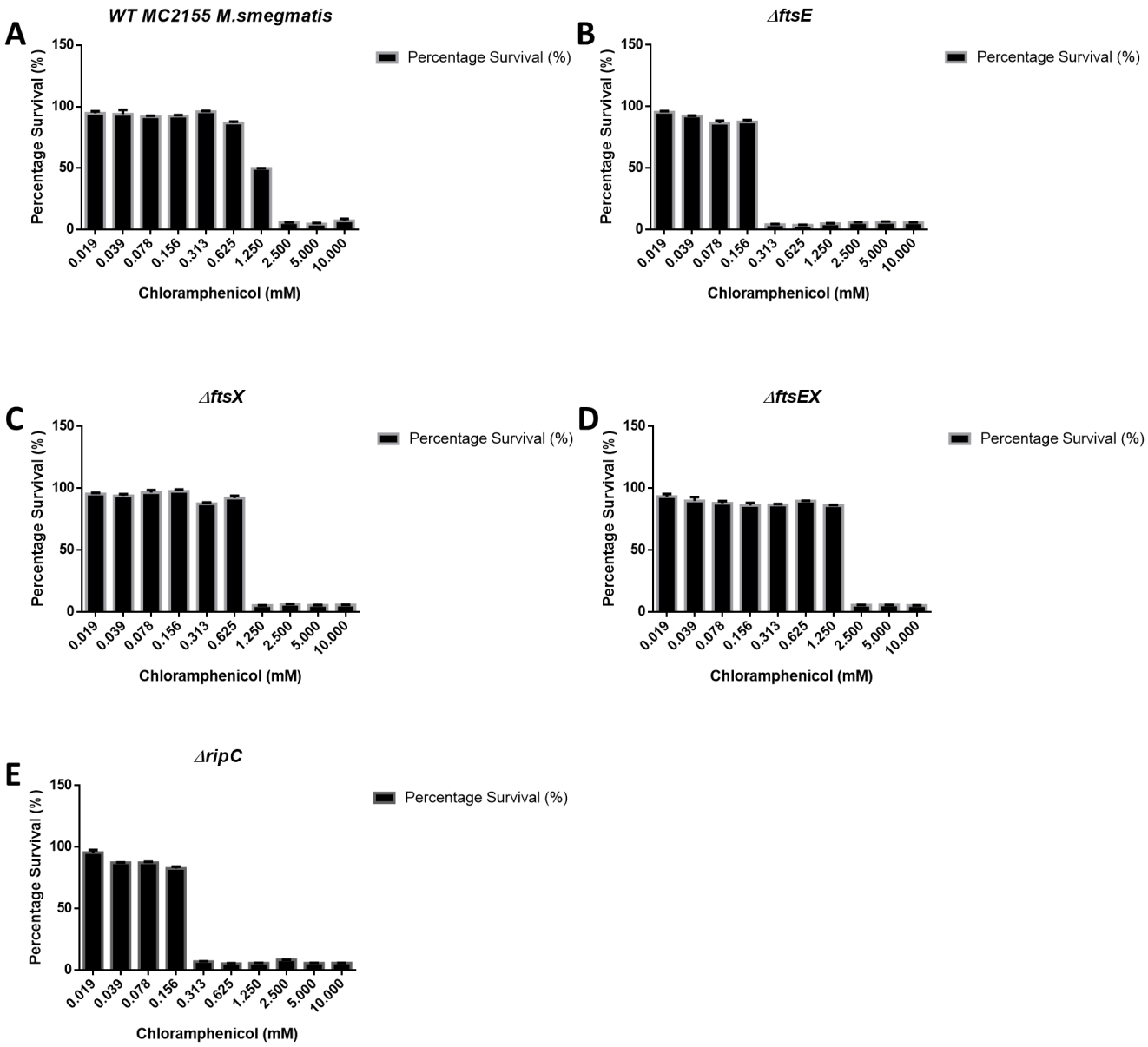

Figure 5. 10. **Survival of *M. smegmatis* against chloramphenicol drug.** Each bar represents the relative fluorescence percentage (%) calculated from the RFU values determined by Alamar blue MIC assay against chloramphenicol drug. Percentage survival was determined for each strain at corresponding concentration (s). Raw RFU data were divided by the average of the cells only control and multiplied by 100 to get the percentage inhibition. Percentage survival were tallied by subtracting the percentage inhibition from 100. The error bars represent standard error of the mean (SEM) derived from duplicates. (A) WT *M. smegmatis MC²155*, (B) *ΔftsE*, (C) *ΔftsX*, (D) *ΔftsEX*, (E) *ΔripC*.

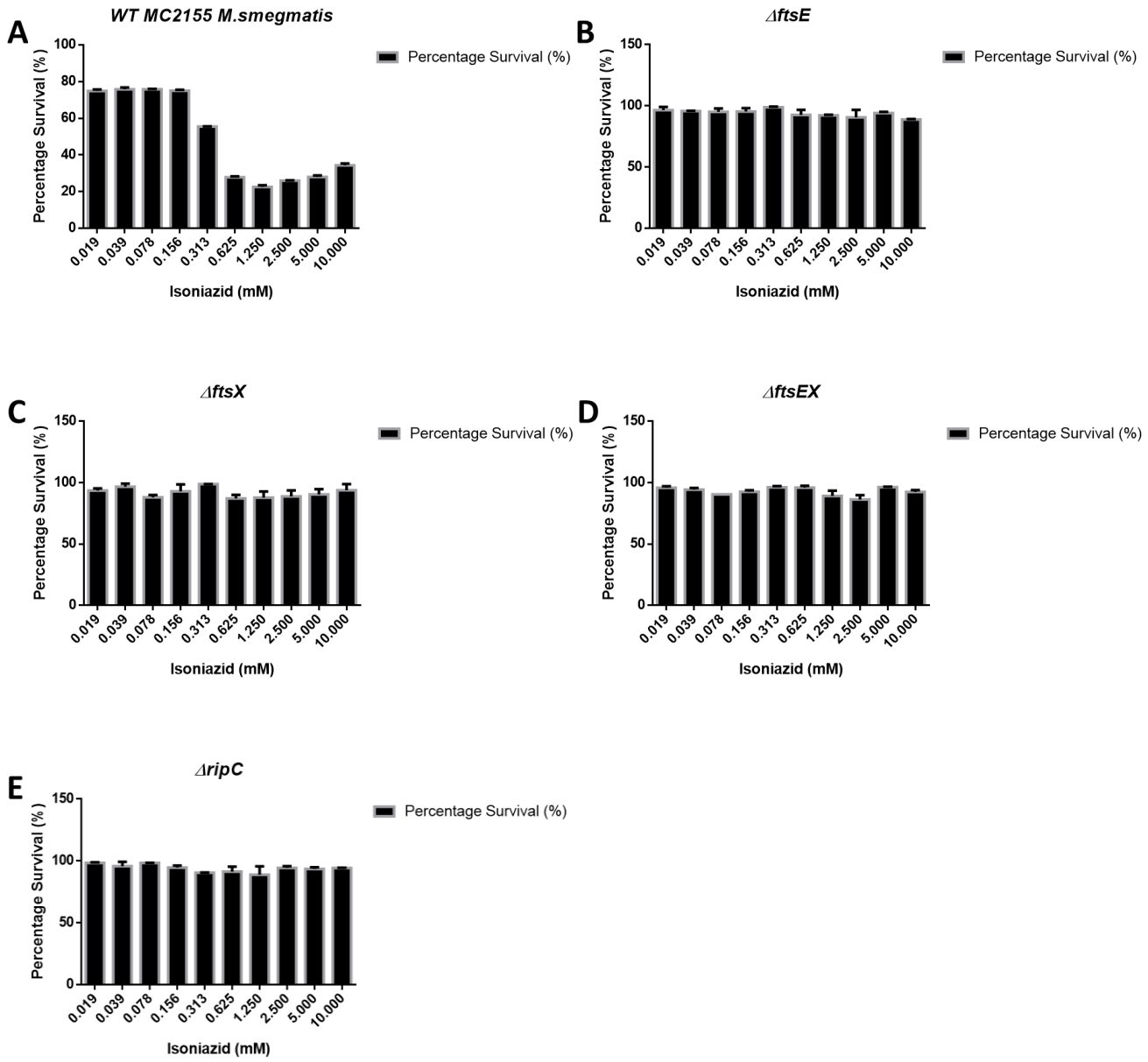

Figure 5. 11. **Percentage Survival against isoniazid drug using *M. smegmatis*.** Each bar represents the relative fluorescence percentage (%) calculated from the RFU values determined by Alamar blue MIC assay against isoniazid drug. Percentage survival was determined for each strain at corresponding concentration (s). Raw RFU data were divided by the average of the cells only control and multiplied by 100 to get the percentage inhibition. Percentage survival were tallied by subtracting the percentage inhibition from 100. The error bars represent standard error of the mean (SEM) derived from duplicates. (A) WT *M. smegmatis MC²155*, (B) *ΔftsE*, (C) *ΔftsX*, (D) *ΔftsEX*, (E) *ΔripC*.

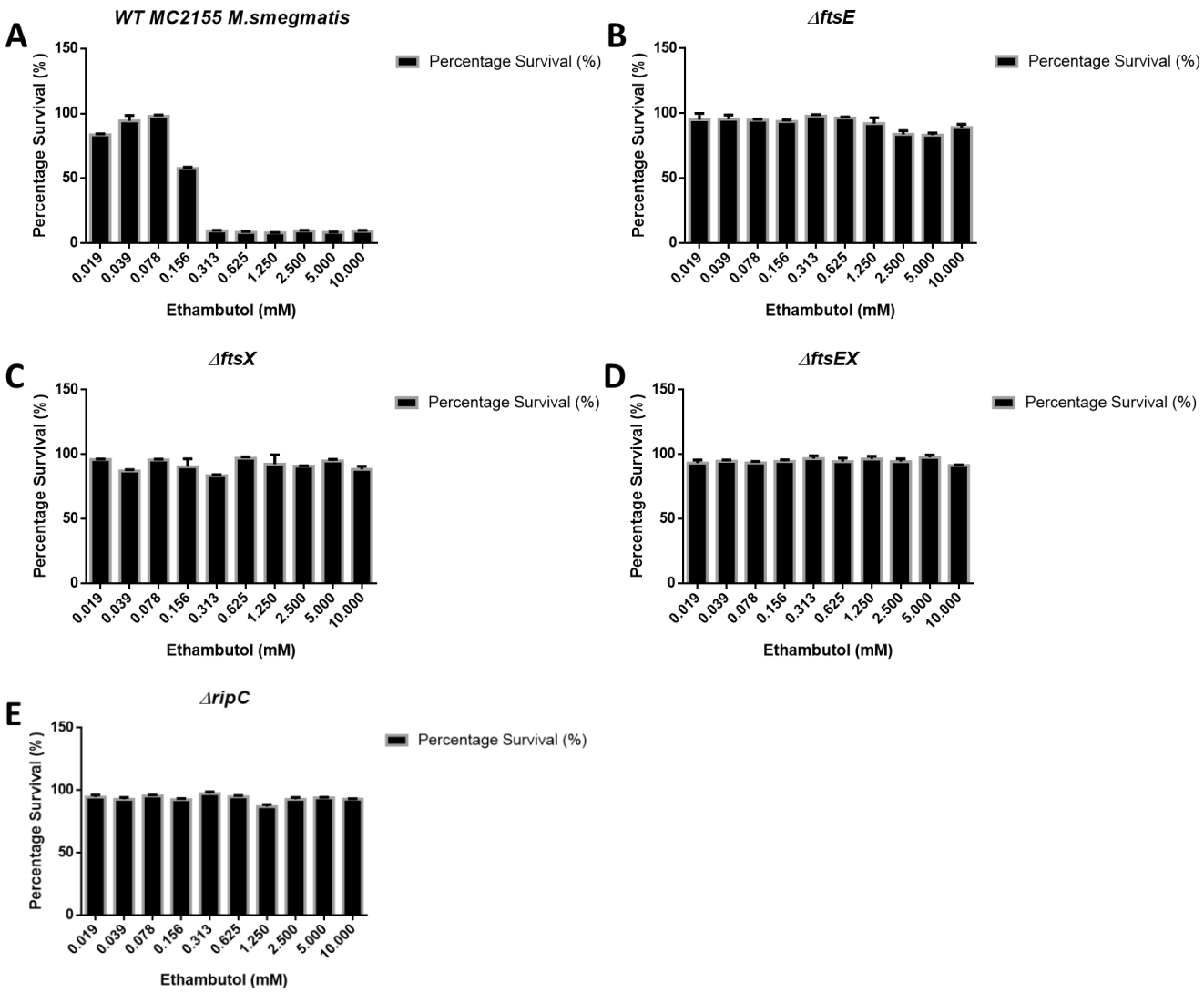

Figure 5. 12. **Percentage survival of *M. smegmatis* against ethambutol drug.** Each bar represents the relative fluorescence percentage (%) calculated from the RFU values determined by Alamar blue MIC assay against ethambutol drug. Percentage survival was determined for each strain at corresponding concentration (s). Raw RFU data were divided by the average of the cells only control and multiplied by 100 to get the percentage inhibition. Percentage survival were tallied by subtracting the percentage inhibition from 100. The error bars represent standard error of the mean (SEM) derived from duplicates. (A) WT *M. smegmatis MC²155*, (B) *ΔftsE*, (C) *ΔftsX*, (D) *ΔftsEX*, (E) *ΔripC*.

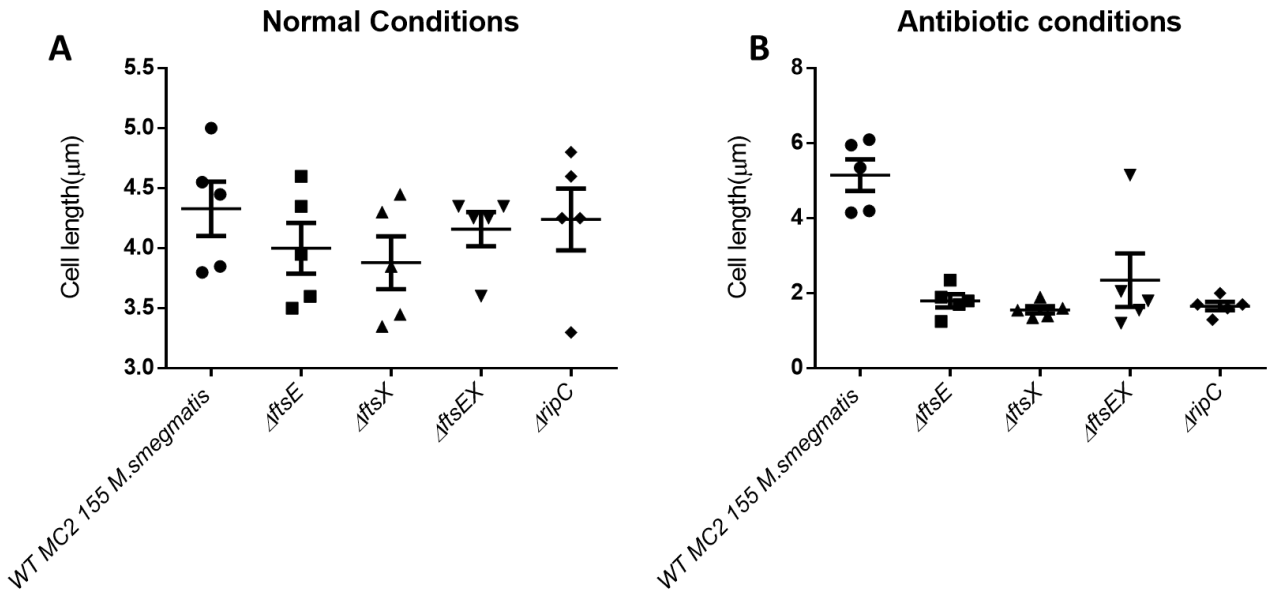

Figure 5. 13. **Scatter plot analysis of *M. smegmatis* showing cell lengths.** (A) Comparison of WT *M. smegmatis MC²155*, *ΔftsE*, *ΔftsX*, *ΔftsEX* and *ΔripC* cell length(s) under normal 7H9 media conditions. (B) Variation in cell length(s) of WT *M. smegmatis MC²155*, *ΔftsE*, *ΔftsX*, *ΔftsEX* and *ΔripC* under antibiotic conditions using rifampicin drug. Concentration of rifampicin drug was 1mM. Cell lengths were enumerated from scanning electron microscopy images (results section). The error bars represent standard error of the mean (SEM) derived from replicates.

Bibliography

1. Barter DM, Agboola SO, Murray MB, Bärnighausen T. Tuberculosis and poverty: The contribution of patient costs in sub-Saharan Africa - A systematic review. Vol. 12, BMC Public Health. 2012.

2. Sulis G, Roggi A, Matteelli A, Raviglione MC. Tuberculosis: Epidemiology and control. Vol. 6, Mediterranean Journal of Hematology and Infectious Diseases. 2014.

3. Mavrici D, Marakalala MJ, Holton JM, Prigozhin DM, Gee CL, Zhang YJ, et al. Mycobacterium tuberculosis FtsX extracellular domain activates the peptidoglycan hydrolase, RipC. Proc Natl Acad Sci U S A [Internet]. 2014;111(22):8037–42. Available from: http://www.pnas.org/cgi/content/long/111/22/8037

4. World Health Organization (WHO). World TB Day 2018 [Internet]. 2018 [cited 2019 Jun 23]. Available from: https://www.gov.za/speeches/world-tb-day-2018-30-nov-2017-1109

5. Kanabus A. TBFACTS.ORG [Internet]. 2018. Available from: https://www.tbfacts.org/tb-statistics-south-africa/

6. World Health Organization (WHO). TUBERCULOSIS (TB) FACT SHEET [Internet]. 2018 [cited 2020 Feb 2]. Available from: https://www.thoracic.org/about/global-public-health/firs/resources/tb-factsheet-firs-2018.pdf

7. Kumar P. Adult pulmonary tuberculosis as a pathological manifestation of hyperactive antimycobacterial immune response. Clin Transl Med. 2016;

8. Centers for Disease Control and Prevention. Latent TB Infection and TB Disease [Internet]. 2016 [cited 2019 Jun 24]. Available from: https://www.cdc.gov/tb/topic/basics/tbinfectiondisease.htm

9. Houben RMGJ, Dodd PJ. The Global Burden of Latent Tuberculosis Infection: A Re-estimation Using Mathematical Modelling. PLoS Med. 2016;

10. Tang P and JJ. Treatment of Latent Tuberculosis Infection. Springer [Internet].

2017;9(4):371–9. Available from: https://www.ncbi.nlm.nih.gov/pmc/articles/PMC5719124/

11. Kieser KJ, Rubin EJ. How sisters grow apart: mycobacterial growth and division. Nat Rev Microbiol [Internet]. 2014;12(8):550–62. Available from: http://www.ncbi.nlm.nih.gov/pubmed/24998739%5Cnhttp://www.nature.com.ezproxy3.lhl.uab.edu/nrmicro/journal/v12/n8/pdf/nrmicro3299.pdf

12. ASalomonPhDah NAmNsNhJw. Progression from latent infection to active disease in dynamic tuberculosis transmission models: a systematic review of validity of modelling assumptions. Lancet Infect Dis. 2018;18(8):1473–3099.

13. Forget, E. J., and Menzies D. Adverse reactions to first-line antituberculosis drugs. Expert Opin Drug Saf [Internet]. 2013;5(2):231–49. Available from: http://sci-hub.tw/https://www.ncbi.nlm.nih.gov/pubmed/16503745

14. Nagarajan S, Whitaker P. Management of adverse reactions to first-line tuberculosis antibiotics. Current Opinion in Allergy and Clinical Immunology. 2018.

15. Palomino J, Martin A. Drug Resistance Mechanisms in Mycobacterium tuberculosis. Antibiotics. 2014;

16. Centers for Disease Control and Prevention. TB Elimination Extensively Drug-Resistant Tuberculosis (XDR TB) [Internet]. 2016 [cited 2019 Nov 10]. Available from: https://www.cdc.gov/tb/publications/factsheets/drtb/xdrtb.htm

17. World Health Organization. WHO | Tuberculosis. World Health Organization. 2017.

18. Palomino J, Martin A. Tuberculosis Clinical Trial Update and the Current Anti-Tuberculosis Drug Portfolio. Curr Med Chem. 2013;

19. World Health Organization (WHO). Tuberculosis (TB), Drug-resistant TB: XDR-TB FAQ [Internet]. 2019 [cited 2019 Nov 14]. Available from: https://www.who.int/tb/areas-of-work/drug-resistant-tb/xdr-tb-faq/en/

20. Mahla Singh Ranjeet. Prevalence of drug-resistant tuberculosis in South Africa. Lancet Infect Dis [Internet]. 2018;18:30401–8. Available from: https://www.thelancet.com/journals/laninf/article/PIIS1473-3099(18)30401-

8/fulltext#articleInformation

21. Orme IM, Basaraba RJ. The formation of the granuloma in tuberculosis infection. Seminars in Immunology. 2014.

22. Amaral EP, Lasunskaia EB, D'Império-Lima MR. Innate immunity in tuberculosis: How the sensing of mycobacteria and tissue damage modulates macrophage death. Microbes and Infection. 2016.

23. Flynn JAL, Chan J. Immune evasion by Mycobacterium tuberculosis: Living with the enemy. Current Opinion in Immunology. 2003.

24. Bhat KH, Yaseen I. Mycobacterium tuberculosis: Macrophage Takeover and Modulation of Innate Effector Responses. In: Mycobacterium - Research and Development. 2018.

25. Ehrt S, Schnappinger D. Mycobacterial survival strategies in the phagosome: Defence against host stresses. Cellular Microbiology. 2009.

26. Zhang YJ, Reddy MC, Ioerger TR, Rothchild AC, Dartois V, Schuster BM, et al. Tryptophan Biosynthesis Protects Mycobacteria from CD4 T-Cell-Mediated Killing. Cell. 2013;155(6):1296–308.

27. Queval CJ, Brosch R, Simeone R. The macrophage: A disputed fortress in the battle against Mycobacterium tuberculosis. Frontiers in Microbiology. 2017.

28. Marakalala MJ, Ndlovu H. Signaling C-type lectin receptors in antimycobacterial immunity. PLoS Pathogens. 2017.

29. Cambier CJ, Falkow S, Ramakrishnan L. Host evasion and exploitation schemes of Mycobacterium tuberculosis. Cell. 2014.

30. Singh A, Crossman DK, Mai D, Guidry L, Voskuil MI, Renfrow MB, et al. Mycobacterium tuberculosis WhiB3 Maintains redox homeostasis by regulating virulence lipid anabolism to modulate macrophage response. PLoS Pathog. 2009;

31. Garcia-Vilanova A, Chan J, Torrelles JB. Underestimated Manipulative Roles of Mycobacterium tuberculosis Cell Envelope Glycolipids During Infection. Frontiers in Immunology. 2019.

32. Neyrolles O, Wolschendorf F, Mitra A, Niederweis M. Mycobacteria, metals, and the macrophage. Immunol Rev. 2015;

33. Wong D, Bach H, Sun J, Hmama Z, Av-Gay Y. Mycobacterium tuberculosis protein tyrosine phosphatase (PtpA) excludes host vacuolar-H +-ATPase to inhibit phagosome acidification. Proc Natl Acad Sci U S A. 2011;

34. Ehrt S, Rhee K, Schnappinger D. Mycobacterial genes essential for the pathogen's survival in the host. Immunol Rev. 2015;264(1):319–26.

35. Jamwal S V., Mehrotra P, Singh A, Siddiqui Z, Basu A, Rao KVS. Mycobacterial escape from macrophage phagosomes to the cytoplasm represents an alternate adaptation mechanism. Sci Rep. 2016;

36. Jr, C.A., Travers, P. and Walport M. Pathogens have evolved various means of evading or subverting normal host defenses. In: Immunobiology: The Immune System in Health and Disease [Internet]. 5th editio. New York: Janeway; 2001. Available from: https://www.ncbi.nlm.nih.gov/books/NBK10757/?term=evolved+various+means+of+evading+or+subverting+normal+host+defense

37. Ehrt S, Schnappinger D. Mycobacterial survival strategies in the phagosome: Defence against host stresses. Vol. 11, Cellular Microbiology. 2009. p. 1170–8.

38. Monika Jankute, Jonathan A.G.Cox, James Harrison and GSB. Assembly of the Mycobacterial Cell Wall. Annu Rev Microbiol [Internet]. 2015;69:405–23. Available from: https://www.annualreviews.org/doi/full/10.1146/annurev-micro-091014-104121?url_ver=Z39.88-2003&rfr_id=ori%3Arid%3Acrossref.org&rfr_dat=cr_pub%3Dpubmed#_i2

39. Squeglia, Flavia AR and RB. Chemistry of Peptidoglycan in Mycobacterium tuberculosis Life Cycle: An off-the-wall Balance of Synthesis and Degradation. Chem Eur J [Internet]. 2018;24:2533–46. Available from: https://sci-hub.tw/https://www.ncbi.nlm.nih.gov/pubmed/28925518

40. Hett EC, Rubin EJ. Bacterial growth and cell division: a mycobacterial perspective. Microbiol Mol Biol Rev [Internet]. 2008;72(1):126–56, table of

contents. Available from: http://www.ncbi.nlm.nih.gov/pubmed/18322037%5Cnhttp://www.pubmedcentral.nih.gov/articlerender.fcgi?artid=PMC2268284

41. Emilisa Frirdich and Erin C. Gaynor. Peptidoglycan hydrolases, bacterial shape, and pathogenesis. Curr Opin Microbiol [Internet]. 2013;16(6):767–78. Available from: https://www.sciencedirect.com/science/article/pii/S1369527413001562?via%3Dihub

42. Uehara T, Parzych KR, Dinh T, Bernhardt TG. Daughter cell separation is controlled by cytokinetic ring-activated cell wall hydrolysis. EMBO J [Internet]. 2010;29(8):1412–22. Available from: http://www.pubmedcentral.nih.gov/articlerender.fcgi?artid=2868575&tool=pmcentrez&rendertype=abstract

43. Chao MC, Kieser KJ, Minami S, Mavrici D, Aldridge BB, Fortune SM, et al. Protein Complexes and Proteolytic Activation of the Cell Wall Hydrolase RipA Regulate Septal Resolution in Mycobacteria. PLoS Pathog. 2013;9(2).

44. Vermassen A, Leroy S, Talon R, Provot C, Popowska M, Desvaux M. Cell wall hydrolases in bacteria: Insight on the diversity of cell wall amidases, glycosidases and peptidases toward peptidoglycan. Frontiers in Microbiology. 2019.

45. Arrigucci R, Pozzi G. Identification of the chain-dispersing peptidoglycan hydrolase LytB of Streptococcus gordonii. PLoS One. 2017;

46. Bajaj R, Bruce KE, Davidson AL, Rued BE, Stauffacher C V., Winkler ME. Biochemical characterization of essential cell division proteins FtsX and FtsE that mediate peptidoglycan hydrolysis by PcsB in Streptococcus pneumoniae. Microbiologyopen. 2016;5(5):738–52.

47. Cascales YGS. Measure of Peptidoglycan Hydrolase Activity. Springer [Internet]. 2017;1615:151–8. Available from: https://link.springer.com/protocol/10.1007%2F978-1-4939-7033-9_12

48. Tanneke Den Blaauwen, Nienke Buddelmeijer, Mirjam E. G. Aarsman CMH

and NN. Timing of FtsZ Assembly in Escherichia coli. J Bacteriol [Internet]. 1999;181(17):5167–75. Available from: https://www.ncbi.nlm.nih.gov/pmc/articles/PMC94019/

49. Sham L-T, Barendt SM, Kopecky KE, Winkler ME. Essential PcsB putative peptidoglycan hydrolase interacts with the essential FtsXSpn cell division protein in Streptococcus pneumoniae D39. Proc Natl Acad Sci U S A [Internet]. 2011;108(45):E1061-9. Available from: http://www.pubmedcentral.nih.gov/articlerender.fcgi?artid=3215045&tool=pmcentrez&rendertype=abstract

50. Meisner J, Montero Llopis P, Sham LT, Garner E, Bernhardt TG, Rudner DZ. FtsEX is required for CwlO peptidoglycan hydrolase activity during cell wall elongation in Bacillus subtilis. Mol Microbiol. 2013;89(6):1069–83.

51. Yang DC, Peters NT, Parzych KR, Uehara T, Markovski M, Bernhardt TG. An ATP-binding cassette transporter-like complex governs cell-wall hydrolysis at the bacterial cytokinetic ring. Proc Natl Acad Sci U S A [Internet]. 2011;108(45):E1052-60. Available from: http://www.pnas.org/content/108/45/E1052.full

52. Schmidt KL, Peterson ND, Kustusch RJ, Wissel MC, Graham B, Phillips GJ, et al. A Predicted ABC Transporter, FtsEX, Is Needed for Cell Division in Escherichia coli. J Bacteriol. 2004;186(3):785–93.

53. Meier EL, Daitch AK, Yao Q, Bhargava A, Jensen GJ, Goley ED. FtsEX-mediated regulation of the final stages of cell division reveals morphogenetic plasticity in Caulobacter crescentus. PLoS Genet. 2017;13(9).

54. Reddy M. Role of FtsEX in cell division of Escherichia coli: Viability of ftsEX mutants is dependent on functional SufI or high osmotic strength. J Bacteriol. 2007;189(1):98–108.

55. Arends SJR, Kustusch RJ, Weiss DS. ATP-binding site lesions in FtsE impair cell division. J Bacteriol. 2009;191(12):3772–84.

56. Cirillo .J. D W. T. and JW. Efficient Electro-transformation of Mycobacterium smegmatis [Internet]. Bio-rad Laboratories Life Science Research. 2000 [cited

2019 Nov 19]. p. 1–4. Available from: https://www.bio-rad.com/en-za/SearchResults?Text=efficient+electro-transformation+of+mycobacterium+smegmatis

57. Franzblau SG, Degroote MA, Cho SH, Andries K, Nuermberger E, Orme IM, et al. Comprehensive analysis of methods used for the evaluation of compounds against Mycobacterium tuberculosis. Tuberculosis. 2012;

58. Jorgensen JH, Turnidge JD. Antibacterial susceptibility tests: dilution and disk diffusion methods. In: Manual of clinical microbiology. 2007.

59. Ollinger J, Bailey MA, Moraski GC, Casey A, Florio S, Alling T, et al. A Dual Read-Out Assay to Evaluate the Potency of Compounds Active against Mycobacterium tuberculosis. PLoS One. 2013;

60. Bertranda RL. Lag phase is a dynamic, organized, adaptive, and evolvable period that prepares bacteria for cell division. Journal of Bacteriology. 2019.

61. Singh B, Nitharwal RG, Ramesh M, Pettersson BMF, Kirsebom LA, Dasgupta S. Asymmetric growth and division in Mycobacterium spp.: Compensatory mechanisms for non-medial septa. Mol Microbiol. 2013;

62. Mao XJ, Yan MY, Zhu H, Guo XP, Sun YC. Efficient and simple generation of multiple unmarked gene deletions in Mycobacterium smegmatis. Sci Rep. 2016;

63. Monahan LG, Hajduk I V., Blaber SP, Charles IG, Harry EJ. Coordinating bacterial cell division with nutrient availability: A role for glycolysis. MBio. 2014;

64. Egan AJF, Cleverley RM, Peters K, Lewis RJ, Vollmer W. Regulation of bacterial cell wall growth. FEBS Journal. 2017.

65. Danilchanka O, Pavlenok M, Niederweis M. Role of porins for uptake of antibiotics by Mycobacterium smegmatis. Antimicrob Agents Chemother. 2008;

66. Aertsen A, Michiels CW. Stress and how bacteria cope with death and survival. Critical Reviews in Microbiology. 2004.

67. Wood JM. Bacterial responses to osmotic challenges. Journal of General Physiology. 2015.

68. Sochocka M, Boratyński J. [Osmoregulation--an important parameter of bacterial growth]. Postepy higieny i medycyny doświadczalnej (Online). 2011.

69. Wood JM. Osmosensing by bacteria: signals and membrane-based sensors. Microbiol Mol Biol Rev. 1999;

70. Voskuil MI, Bartek IL, Visconti K, Schoolnik GK. The response of Mycobacterium tuberculosis to reactive oxygen and nitrogen species. Front Microbiol. 2011;

71. Schnappinger D, Ehrt S, Voskuil MI, Liu Y, Mangan JA, Monahan IM, et al. Transcriptional adaptation of Mycobacterium tuberculosis within macrophages: Insights into the phagosomal environment. J Exp Med. 2003;

72. Zhu JH, Wang BW, Pan M, Zeng YN, Rego H, Javid B. Rifampicin can induce antibiotic tolerance in mycobacteria via paradoxical changes in rpoB transcription. Nat Commun. 2018;

73. Sham LT, Jensen KR, Bruce KE, Winkler ME. Involvement of FtsE ATPase and FtsX extracellular loops 1 and 2 in FtsEX-PcsB complex function in cell division of Streptococcus pneumoniae D39. MBio. 2013;4(4).

74. Aldridge BB, Fernandez-Suarez M, Heller D, Ambravaneswaran V, Irimia D, Toner M, et al. Asymmetry and aging of mycobacterial cells lead to variable growth and antibiotic susceptibility. Science (80-). 2012;

75. Heidrich C, Templin MF, Ursinus A, Merdanovic M, Berger J, Schwarz H, et al. Involvement of N-acetylmuramyl-L-alanine amidases in cell separation and antibiotic-induced autolysis of Escherichia coli. Mol Microbiol. 2001;

76. Claessen D, Emmins R, Hamoen LW, Daniel RA, Errington J, Edwards DH. Control of the cell elongation-division cycle by shuttling of PBP1 protein in Bacillus subtilis. Mol Microbiol. 2008;

77. Yang DC, Blair KM, Salama NR. Staying in Shape: the Impact of Cell Shape on Bacterial Survival in Diverse Environments. Microbiol Mol Biol Rev. 2016;

78. Senzani S, Li D, Bhaskar A, Ealand C, Chang J, Rimal B, et al. An Amidase-3 domain-containing N-acetylmuramyl-L-alanine amidase is required for mycobacterial cell division. Sci Rep. 2017;

79. Senzani S. Characterisation of mycobacterial amidases and their role in bacterial growth and physiology [Internet]. Univeristy of Witwatersrand; 2018. Available from: https://hdl.handle.net/10539/25446

80. Rojas E, Theriot JA, Huang KC. Response of Escherichia coli growth rate to osmotic shock. Proc Natl Acad Sci U S A. 2014;

81. Claessen D, Errington J. Cell Wall Deficiency as a Coping Strategy for Stress. Trends in Microbiology. 2019.

82. Ultee E, Ramijan K, Dame RT, Briegel A, Claessen D. Stress-induced adaptive morphogenesis in bacteria. Adv Microb Physiol. 2019;

83. Prashar A, Bhatia S, Gigliozzi D, Martin T, Duncan C, Guyard C, et al. Filamentous morphology of bacteria delays the timing of phagosome morphogenesis in macrophages. J Cell Biol. 2013;

84. Chauhan A, Lofton H, Maloney E, Moore J, Fol M, Madiraju MVVS, et al. Interference of Mycobacterium tuberculosis cell division by Rv2719c, a cell wall hydrolase. Mol Microbiol. 2006;

85. Parthasarathy, G., Lun, S., Guo, H., Ammerman, N.C., Geiman, D.E., Bishai W. Rv2190c, an NlpC/P60 Family Protein, Is Required for Full Virulence of Mycobacterium tuberculosis. PLoS One [Internet]. 2012;7(8):1–8. Available from: https://www.ncbi.nlm.nih.gov/pmc/articles/PMC3432046/pdf/pone.0043429.pdf

86. Hartmann M, Berditsch M, Hawecker J, Ardakani MF, Gerthsen D, Ulrich AS. Damage of the bacterial cell envelope by antimicrobial peptides gramicidin S and PGLa as revealed by transmission and scanning electron microscopy. Antimicrob Agents Chemother. 2010;

87. Biswas D, Tiwari M, Tiwari V. Molecular mechanism of antimicrobial activity of chlorhexidine against carbapenemresistant Acinetobacter baumannii. PLoS One. 2019;

88. Wolf AJ, Liu GY, Underhill DM. Inflammatory properties of antibiotic-treated bacteria. J Leukoc Biol. 2017;

89. Cheung HY, Wong MMK, Cheung SH, Liang LY, Lam YW, Chiu SK.

Differential actions of chlorhexidine on the cell wall of bacillus subtilis and escherichia coli. PLoS One. 2012;

90. Odermatt PD, Hannebelle MTM, Eskandarian HA, Nievergelt AP, McKinney JD, Fantner GE. Overlapping and essential roles for molecular and mechanical mechanisms in mycobacterial cell division. Nature Physics. 2019.

91. Dahl JL. Electron microscopy analysis of Mycobacterium tuberculosis cell division. FEMS Microbiol Lett. 2004;

92. Yadav AK, Espaillat A, Cava F. Bacterial strategies to preserve cell wall integrity against environmental threats. Frontiers in Microbiology. 2018.

93. Deng S, Sun J, Zhao R, Ding M, Zhang Y, Sun Y, et al. Populus euphratica APYRASE2 enhances cold tolerance by modulating vesicular trafficking and extracellular ATP in arabidopsis plants. Plant Physiol. 2015;

94. Muchová K, Wilkinson AJ, Barák I. Changes of lipid domains in Bacillus subtilis cells with disrupted cell wall peptidoglycan. FEMS Microbiol Lett. 2011;

95. Yamada H, Yamaguchi M, Igarashi Y, Chikamatsu K, Aono A, Murase Y, et al. Mycolicibacterium smegmatis, Basonym Mycobacterium smegmatis, Expresses Morphological Phenotypes Much More Similar to Escherichia coli Than Mycobacterium tuberculosis in Quantitative Structome Analysis and CryoTEM Examination. Front Microbiol. 2018;

96. Vijay S, Anand D, Ajitkumar P. Unveiling unusual features of formation of septal partition and constriction in mycobacteria-an ultrastructural study. J Bacteriol. 2012;

97. Zuber B, Chami M, Houssin C, Dubochet J, Griffiths G, Daffé M. Direct visualization of the outer membrane of mycobacteria and corynebacteria in their native state. J Bacteriol. 2008;